Contrib Mineral Petrol (1994) 117:375–393

Daniel Vielzeuf · Jean Marc Montel

Partial melting of metagreywackes. Part I. Fluid-absent experiments and phase relationships

Received: 21 June 1993 / Accepted: 8 April 1994

Abstract Island arcs, active and passive margins are the best tectonic settings to generate fertile reservoirs likely to be involved in subsequent granitoid genesis. In such environments, greywackes are abundant crustal rock types and thus are good candidates to generate large quantities of granitoid magmas. We performed a series of experiments, between 100 and 2000 MPa, on the fluid-absent melting of a quartz-rich aluminous metagreywacke composed of 32 wt% plagioclase (Pl) (An_{22}), 25 wt% biotite (Bt) ($X_{Mg}45$), and 41 wt% quartz (Qtz). Eighty experiments, averaging 13 days each, were carried out using a powder of minerals (≤ 5 μm) and a glass of the same composition. The multivariant field of the complex reaction Bt + Pl + Qtz ⇔ Grt/Crd/Spl + Opx + Kfs + melt limited by the Opx-in and Bt-out curves, is located between 810–860°C at 100 MPa, 800–850°C at 200 MPa, 810–860°C at 300 MPa, 820–880°C at 500 MPa, 860–930°C at 800 MPa, 890–990°C at 1000 MPa, and at a temperature lower than 1000°C at 1500 and 1700 MPa. The melting of biotite + plagioclase + quartz produced melt + orthopyroxene (Opx) + cordierite (Crd) or spinel (Spl) at 100, 200 and 300 MPa, and melt + orthopyroxene + garnet (Grt) from 500 to 1700 MPa (+ Qtz, Pl, FeTi Oxide at all pressures). K-feldspar (Kfs) was found as a product of the reaction in some cases and we observed that the residual plagioclase was always strongly enriched in orthoclase component. The *P-T* surface corresponding to the multivariant field of this reaction is about 50 to 100°C wide. At temperatures below the appearance of orthopyroxene, biotite is progressively replaced by garnet with increasing *P*. At 850°C, we observed that (1) the modal proportion of garnet increases markedly with *P*; (2) the grossular content of the garnet increases regularly from about 4 mol% at 500 MPa to 15 mol% at 2000 MPa. These changes can be ascribed to the reaction Bt + Pl + Qtz ⇔ Grt + Kfs + melt with biotite + plagioclase + quartz on the low-*P* side of the reaction. As a result, at 2000 MPa, we observed the progressive disappearance of biotite without production of orthopyroxene. These experiments emphasize the importance of this reaction for the understanding of partial melting processes and evolution of the lower continental crust. Ca-poor Al-metagreywackes represent fertile rocks at commonly attainable temperatures (i.e. 800–900°C), below 700 MPa. There, 30 to 60 vol.% of melt can be produced. Above this pressure, temperatures above 900°C are required, making the production of granitoid magmas more difficult. Thin layers of gneisses composed of orthopyroxene, garnet, plagioclase, and quartz (± biotite), interbedded within sillimanite-bearing paragneisses, are quite common in granulite terrains. They may result from partial melting of metagreywackes and correspond to recrystallized mixtures of crystals (+ trapped melt) left behind after removal of a major proportion of melt. Available experimental constraints indicate that extensive melting of pelites takes place at a significantly lower temperature (850°C ± 20) than in Al-metagreywackes (950°C ± 30), at 1000 MPa. The common observation that biotite is no longer stable in aluminous paragneisses while it still coexists commonly with orthopyroxene, garnet, plagioclase and quartz, provides rather tight temperature constraints for granulitic metamorphism.

D. Vielzeuf ✉ J.M. Montel
Département de Géologie,
URA 10 du CNRS, 5 rue Kessler,
F-63038 Clermont-Ferrand, France
Editorial responsibility: W. Schreyer

Introduction

Partial melting and the ascent of granitoid magmas are among the main processes leading to internal differentiation of the continental crust. In the absence of satisfactory thermodynamic models to calculate the compositions of silicic melts in complex systems, as a function of bulk composition, pressure and temperature, a systematic review of fluid-absent partial melting of the most common crustal lithologies has been undertaken for the

last ten years by various authors (see Vielzeuf et al. 1990 and Skjerlie and Johnston 1992 for reviews).

Island arcs, active and passive margins are among the best tectonic environments to generate fertile reservoirs likely to be involved in subsequent granitoid genesis (Vielzeuf et al. 1990). In such environments, greywackes are abundant crustal rock types and thus are probably better candidates than pelites as sources for large volumes of granitoid magmas (Clemens and Wall 1981; Miller 1985). Such are the inferred source rocks for the S-type granitoids in the Lachlan Fold Belt (Clemens and Wall 1981 1984; Chappell 1984; White and Chappell 1988) and the Massif Central in the Hercynian Belt (Pin and Duthou 1990).

Some significant studies on the fluid-absent melting of metagreywackes are already available (Rutter and Wyllie 1988; Skjerlie and Johnston 1992). These deal with rocks of intermediate composition (metatonalite) involving hornblende and plagioclase with An contents close to An_{40}. So far, only a limited number of experiments have been carried out on peraluminous metagreywackes, and those available have been performed under fluid-present (water-saturated or undersaturated) conditions (Hoschek 1976; Hoffer and Grant 1980; Conrad et al. 1988). The reaction biotite + plagioclase + quartz = orthopyroxene + garnet (or cordierite) + K-feldspar + melt has been suggested as a model reaction for the fluid-absent partial melting of such rocks (Thompson 1982; Clemens 1984; Grant 1985; Vielzeuf and Holloway 1988). In order to investigate this hypothesis, a series of experiments was performed between 100 and 2000 MPa on a Ca-poor aluminous metagreywacke composed of biotite + plagioclase (An_{22}) + quartz. The aim was to determine the exact nature and *P-T* location of the reaction, and the width of the multivariant field. In a complementary paper (J.M. Montel and D. Vielzeuf, in preparation) we will discuss the compositions and the proportions of the phases (and especially the melts) as a function of *P* and *T*.

Experimental techniques

Starting material

The starting material is a natural quartz-rich metagreywacke composed of quartz (40 wt%), An_{22} plagioclase (32 wt%), and biotite (25 wt%), with minor apatite, zircon, monazite, tourmaline, and pyrite. The chemical compositions of the whole rock and its constitutive minerals are reported in Table 1. The modal proportions of the minerals were determined by mass balance calculations, while the water content of the sample was determined by wet chemical methods (Karl-Fischer titration).

The sample (CEV) was collected in the so-called "Série Cévenole" (Marignac et al. 1980) in the vallée de la Beaume, Ardèche, France. This metamorphic series consists of metapelites

Table 1 Compositions and CIPW norms of the starting materials and some greywackes. Compositions of the biotite and plagioclase from CEVP. (*CEVP* composition of the powder, *CEVG* composition of the glass prepared from CEVP, *GW* average greywacke, Pettijohn 1963, *HGW* average Harz greywacke, Pettijohn 1963, *CRS* average Columbia River Sand, Whetten et al. 1969). CEVP analysed by ICP, wet chemical methods (CO_2, B, F, FeO/Fe_2O_3, S), and Karl-Fischer titration for H_2O at CRPG, Nancy, France. CEVG, biotite, and plagioclase analysed by microprobe

	CEVP	CEVG	GW	HGW	CRS		Biotite	Plagioclase	
SiO_2	69.99	69.03	66.70	69.70	66.50		35.63	63.24	
Al_2O_3	12.96	12.96	13.50	14.30	13.90		19.51	23.55	
Fe_2O_3	0.45	–	1.60	1.90	4.70		–	–	
FeO	4.42	4.17	3.50	2.40			20.62	0.06	
MgO	2.36	2.14	2.10	1.80	2.00		9.13	0.01	
MnO	0.06	0.08	–	–	–		0.22	0.00	
CaO	1.67	1.64	2.50	1.30	3.40		0.00	4.76	
Na_2O	2.95	2.70	2.90	3.10	2.90		0.16	8.99	
K_2O	2.41	2.45	2.00	1.40	2.10		9.29	0.37	
TiO_2	0.70	0.81	–	–	–		2.80	0.00	
P_2O_5	0.20	–	–	–	–		–	–	
CO_2	0.10	–	1.20	0.90	–		–	–	
H_2O	1.43	–	–	–	–		–	–	
F	0.09	–	–	–	–		–	–	
S	0.067	–	–	–	–		–	–	
B	<20 ppm	–	–	–	–		–	–	
Total	99.86	95.98	96.00	96.80	95.50		97.36	100.98	
Qtz	34.52	35.85	34.64	42.01	31.33	Si	5.55	Si	2.78
Crn	3.37	3.00	4.80	7.41	0.67	Al^{IV}	2.45	Al	1.22
Or	14.24	15.11	11.82	8.27	12.41				
Ab	24.96	23.79	24.54	26.23	24.54	Al^{VI}	1.13	Na	0.76
An	5.82	8.49	4.82	0.76	16.87	Fe	2.68	K	0.02
En	5.88	5.58	5.23	4.48	4.98	Mg	2.13	Ca	0.22
Fs	6.70	6.58	4.49	3.60	3.85	Ti	0.33		
Mag	0.65	–	2.32	2.75	–	Mn	0.03	Ab	0.757
Ilm	1.33	1.60	–	–	–			Or	0.021
Hem	–	–	–	–	4.70	K	1.85	An	0.222
Ap	0.47	–	–	–		Na	0.05		
Fl	0.15	–	–	–	–				
Cal	0.23		2.73	2.05	–				
*X*Mg	0.47	0.48	0.43	0.44	0.46		0.44		

(Bt + Sil + Qtz + Pl ± Crd), with minor intercalations of sillimanite-free metagreywackes which provided our starting material. The series has been affected by a low-pressure, high-temperature metamorphic event of Hercynian age at about 300 Ma. A geothermobarometric study, carried out on adjacent rocks (Montel et al. 1986), indicates *P-T* conditions of metamorphism of about 200–320 MPa and 680–710°C. The fact that the rock was originally equilibrated at low pressure is important and will be helpful in interpreting our experimental results. The rocks show textural evidence of incipient anatexis (Weber and Barbey 1986) except in the metagreywackes. We attribute this difference to the absence of Al-silicate in these rocks.

This sample was selected for two major reasons:

1. As stressed by White and Chappell (1988), most greywackes are slightly peraluminous. Our starting material has about 3% normative corundum and is very close to the average greywacke composition of Pettijohn (1963) (see Table 1).

2. The mineralogical composition of our starting material is remarkably simple (biotite + plagioclase + quartz) allowing a direct test of the fluid-absent melting reactions proposed in petrogenetic models. In order to isolate the effects of the various chemical components, a relatively Ca-poor sample was selected to prevent extensive amphibole crystallization.

Two different starting materials were used in order to reverse the equilibria:

1. A very fine *rock powder* (CEVP – grain size $\leq$ 5 μm) was obtained by repeated grinding, in an agate mortar under alcohol, and checked under the microscope. Special attention was paid to this stage to ensure the best conditions to reach equilibrium.

2. A *glass* of the same bulk composition (CEVG) was obtained by melting the powder in a sealed platinum capsule at 300 MPa, 1300°C for 30 min. The crystal-free glass was subsequently ground in an agate mortar to get particles varying in size from 50 to 150 μm. Microprobe analyses of the glass were obtained (Table 1) and indicate no major difference between the glass and the powder.

Thin-walled Au capsules (3 mm OD × 2.6 mm ID × 10 mm long) were welded shut at one end and loaded with about 0.01 g of starting material kept in a dessicator and dried at 110°C for at least 2 h before loading. For the piston-cylinder experiments, the capsules were squashed flat and folded into "packets" with approximate dimensions of 3.5 × 5 × 0.6 mm. These packets lay flat in the pressure cells so that the samples would experience the minimum possible thermal gradients. Thirteen days was the average duration of the runs.

Apparatus

Experimental procedures are similar to those described by Vielzeuf and Clemens (1992). The lower-pressure experiments ($P \leq 300$ MPa) were run in cold-seal vessels with vertically mounted furnaces (hot spot on top), and used N_2 (with trace H_2O) as the pressure medium. Temperatures were measured with external, type-S thermocouples calibrated against the melting point of NaCl (801°C), $SrCl_2$ (875°C), and Ag (963°C), at 1 atm, and are believed accurate to ± 5°C. The difference between the external temperature measured by the thermocouple and the temperature of the sample has been measured at 1 atm using two calibrated thermocouples; it is always less than 3°C. The temperature gradient inside the vessel is less than 2°C over 4 cm. The errors quoted for the cold-seal experiments correspond to the sum of (1) the errors in calibrating the thermocouples (2°C); (2) the temperature gradient along the capsule; (3) the temperature variation during the run. Pressure was monitored using a solid-state transducer accurate to ± 0.6 MPa and regularly checked against a Heise gauge.

Gas-apparatus experiments at 500, 800 and 1000 MPa were carried out in a 1500 MPa, large-volume, internally heated pressure vessel. The vessel was run horizontally, with a pressure medium of N_2, and the samples were heated by a single-zone, platinum resistance furnace. Pressure was measured by a manganin resistance cell. The variation of the pressure during an experiment was always less than 5 MPa, usually less than 2 MPa. We estimate the pressure accuracy to be within ± 10 MPa. Temperature is monitored by a type-S thermocouple located at the contact with the platinum furnace winding. Within the furnace, the temperature is measured by three type-B thermocouples immediately adjacent to each of the capsules and calibrated against the melting point of NaCl, $SrCl_2$, and Ag at 1 atm. The longitudinal temperature gradient is about 2°C/mm, and the variation during an experiment is comprised between 2 and 5 °C. The error reported in Table 2 for each run is calculated by adding the error in the calibration of the thermocouple (± 1°C), the temperature variation during the run, and the gradient along the capsule.

All experiments above 1000 MPa and some at 500, 750, and 1000 MPa were carried out in a non-end-loaded, 1.91 cm, piston-cylinder apparatus. The pressure assemblies were nearly the same as those described by Perkins et al. (1981) and Vielzeuf and Clemens (1992). They comprised an outer NaCl bushing surrounding a glass sleeve, in turn surrounding the graphite furnace. Inside the furnace, an additional glass sleeve, cored by crushable magnesia, served as the pressure medium. At the core, the small flat Au capsule was surrounded by crushed borosilicate glass. A type-C thermocouple, protected by an alumina ceramic, passed through a small hole in the magnesia. The thermocouple tip was protected by a small amount of BN powder and separated from the Au capsule by a thin (< 1 mm) magnesia wafer. Independant temperature calibration experiments suggest that the difference between the temperature at the thermocouple tip and the capsule is less than 5°C. A cold pressure of 150 MPa was initially applied to the assembly. The temperature was then raised to approximately 510°C, at which point the pressure ceased to increase and began to decrease. Then, the desired final pressure could be applied without shattering the cell. No pressure correction was applied. All experiments were simultaneously brought to final *P-T* conditions, and we used the hot piston-in technique.

Observation and analysis of run products

The contents of each capsule were split into different portions. Part was ground, and used to make optical grain mounts examined under the microscope. Another part was mounted as polished slides and studied both optically in reflected light under the microscope and by SEM. Optical observations provided preliminary determination of the phases present but exact determination always needed SEM (with EDS) and microprobe investigations.

Electron probe analyses on polished mounts were carried out on a Cameca Camebax Micro microprobe fitted with a Link energy dispersive system (EDS) for phase identification, at the Centre Régional de Mesures Physiques in Clermont. Images were obtained on a Leica-Cambridge stereoscan 360 SEM. The best results were obtained using backscattered-electron images with an accelerating voltage of 20 kV, a sample current of 2 nA, and a working distance of 17–18 mm.

Description of the run products

Eighty experiments were performed in the range 100 to 2000 MPa and 780 to 1000°C. The results are reported in Table 2 and a selection of the run products are shown in the SEM images of Fig. 1.

In addition to biotite, plagioclase and quartz, several other phases (cordierite, spinel, garnet, orthopyroxene and melt) appeared as a function of pressure and temperature. In some rare cases gedrite and staurolite were detected. Magnetite, Ti-magnetite, ilmenite, and

Table 2 Experimental results *EH* externally heated, cold-seal pressure vessel, *IH* internally heated gas apparatus, *PC* piston cylinder, *S.M.* starting material – powder (*P*) or glass (*G*). *Dur* duration of the experiment, measured from the attainment of the desired temperature to the quench. *Qtz* quartz, *Pl* plagioclase, *Bt* biotite, *Grt* garnet, *Opx* orthopyroxene, *Ged* gedrite, *Mag* magnetite, *Ti-Mag* titano-magnetite, *Ilm* ilmenite, *Rt* rutile, *Op* undifferentiated opaque phase, *Po* Pyrrhotite, *Ap* apatite, *Crd* cordierite, *Hc* hercynite, *St* staurolite, *Kfs* alkali feldspar

Run no.					Phases present
100 Mpa		S.M.	T°C	Dur. (h)	
CE90-2A	EH	P	790 ± 5	255	Qtz, Pl, Bt, Op, (powder)
		G		255	Bt, Hc, Mag, other ?
CE90-2B	EH	P	803 ± 5	255	Qtz, Pl, Bt, Op (powder)
		G		255	?
CE90-2C	EH	P	821 ± 6	255	Qtz, Pl, Bt, Opx, Crd, Mag, Glass
		G		255	?
CE90-2D	EH	P	854 ± 8	255	Qtz, Pl, Bt, Opx, Crd, Mag, Ti-Mag, Glass
		G		255	Bt, Opx, other?
200 Mpa					
CE89-1A	EH	P	782 ± 8	594	Qtz, Pl, Bt (powder)
CE89-1B	EH	P	812 ± 4	592	Qtz, Pl, Bt, Opx, Crd, Mag, Glass
CE89-1C	EH	P	825 ± 7	426	Qtz, Pl, Bt, Opx, Crd, Mag, Glass
CE89-1D	EH	P	859 ± 7	331	Qtz, Pl, Opx, Crd, Mag, Ilm, Glass
300 Mpa					
CE90-6	EH	P	804 ± 5	350	Qtz, Pl, Bt, Op, (Opx, Hc)
		G		350	Qtz, Pl, Bt, Hc, Mag, Po, Glass
CE90-4A	EH	P	805 ± 5	607	Qtz, Pl, Bt, Mag, Ti-Mag, Glass
CE90-3A	EH	P	810 ± 4	346	Qtz, Pl, Bt, Opx, Mag, Po, Glass
CE90-4B	EH	P	833 ± 5	470	Qtz, Pl, Bt, Opx, Crd, Mag, Po, Glass
CE90-3B	EH	G	834 ± 5	352	Qtz, Pl, Bt, Opx, Mag, Hc, Glass
CE90-3C	EH	G	850 ± 5	352	Qtz, Pl, Bt, Opx, Hc, Mag, Ilm, Po, Glass
CE90-4C	EH	P	853 ± 5	351	Qtz, Pl, Bt, Opx, Crd, Mag, Ilm, Po, Glass
		G		351	Qtz, Pl, Bt, Opx, Hc, Mag, Glass
CE90-5	EH	P	875 ± 5	96	Qtz, Pl, Opx, Hc, Ilm, Po, Glass
		G		96	Qtz, Pl, Opx, Hc, Ilm, Po, Glass
500 Mpa					
PC2-91–13	PC	P	800 ± 8	428	Qtz, Pl, Bt, Grt, Glass
A117-C	IH	P	809 ± 11	350	Qtz, Pl, Bt, Grt, Mag, Po, Glass
		G		350	Qtz, Pl, Bt, Hc, Mag, Po, Glass
A99	IH	P	851 ± 7	425	Qtz, Pl, Opx, Mag, Ti-Mag, Glass
		G		425	Qtz, Pl, Bt, Opx, Mag, Ti-Mag, Glass
A117-B	IH	P	867 ± 8	350	Qtz, Pl, Bt, Opx, Grt, Hc, Mag, Glass
		G		350	Qtz, Pl, Bt, Opx, Hc, Mag, Glass
A97	IH	P	883 ± 8	285	Qtz, Pl, Opx, Mag, Ti-Mag, Glass
		G		285	Qtz, Pl, Opx, Hc, Mag, Ti-Mag, Glass
A117-A	IH	P	898 ± 7	350	Qtz, Pl, Opx, Hc, Mag, Po, Glass
750 MPa					
PC1-91–19	PC	P	830 ± 8	412	Qtz, Pl, Bt, Grt, (Glass ?)
800 Mpa					
A118-C	IH	P	805 ± 12	451	Qtz, Pl, Bt, Op, Po, Ged
		G		451	Qtz, Pl, Bt, Hc, Glass
A109-C	IH	P	855 ± 9	305	Qtz, Pl, Bt, Ged, Grt, Ti-Mag, Mag, Glass
A118-B	IH	P	864 ± 11	451	Qtz, Pl, Bt, Opx, Grt, Po, Ilm, Glass
		G		451	Qtz, Pl, Bt, Opx, Grt, Hc, Po, Glass
A115-C	IH	P	875 ± 9	362	Qtz, Pl, Bt, Opx, Grt, Mag, Ti-Mag, Glass
	IH	G		362	Qtz, Pl, Bt, Opx, Grt, Op, Glass
A109-B	IH	P	879 ± 8	305	Qtz, Pl, Bt, Opx, Grt, Ti-Mag, Glass
A109-A	IH	P	886 ± 8	305	Qtz, Pl, Bt, Opx, Grt, Op, Glass
A118-A	IH	P	913 ± 9	451	Qtz, Pl, Bt, Opx, Grt, Mag, Ilm, Glass
		G		451	Qtz, Pl, Bt, Opx, Grt, Ilm, Glass
A115-B	IH	G	919 ± 9	362	Qtz, Pl, Bt, Opx, Grt, (Hc), Ti-Mag, Glass
A115-A	IH	P	942 ± 9	362	Qtz, Pl, Opx, Grt, Ti-Mag, Glass
		G		362	Qtz, Pl, Opx, Ti-Mag, Glass
A104	IH	P	1026 ± 9	306	Qtz, Opx, Ti-Mag, Glass
		G	1040 ± 9	306	Qtz, (Pl ?), Opx, Ti-Mag (?), Glass

Table 2 (continued)

1000 MPa					
A113-C	IH	P	803 ± 13	403	Qtz, Pl, Bt, St, Mag, Ti-Mag, Glas
		G		403	Qtz, Pl, Kfs, Bt, Mag, , Ti-Mag, (Glass ?)
PC2-91-12	PC	P	850 ± 8	333	Qtz, Pl, Bt, Grt, Po, Ap, Glass
A113-B	IH	P	858 ± 11	403	Qtz, Pl, Bt, Grt, Ti-Mag, Glass
		G		403	Qtz, Pl, Bt, Grt, Mag, Ti-Mag, Glass
A114-C	IH	P	860 ± 15	278	Qtz, Pl, Bt, Grt, Ti-Mag, Glass
		G		278	Qtz, Pl, Kfs, Bt, Opx, Op, (Glass ?)
A113-A	IH	P	874 ± 9	403	Qtz, Pl, Bt, Grt, Ti-Mag, Glass
		G		403	Qtz, Pl, Bt, Opx, Grt, Ti-Mag, Glass
A114-B	IH	P	885 ± 14	278	Qtz, Pl, Bt, Grt, Ti-Mag, Glass
		G		278	Qtz, Pl, Bt, Opx, Grt, Mag, Glass
A153-C	IH	P	890 ± 10	120	Qtz, Pl, Kfs, Bt, Grt, Opx, Po, Glass
		G		120	Qtz, Pl, Kfs, Bt, Fe-Ox, Grt, Glass
A120-C	IH	P	922 ± 17	240	Qtz, Pl, Bt, Opx, Grt, (Hc ?), Po, Glass
PC1-91-21	PC	P	930 ± 8	304	Qtz, Pl, Bt, Opx, Grt, Glass
A153-B	IH	P	950 ± 10	120	Qtz, Pl, Kfs, Bt, Grt, Opx, Po, Glass
		G		120	Qtz, Pl, (Kfs), (Bt), Ti-Mag, Grt, Opx, Glass
PCJRH-92-3	PC	P	960 ± 8	293	Qtz, Pl, Bt, Opx, Grt, Glass
PCJRH-92-6	PC	P	960 ± 8	235	Qtz, Pl, Bt, Grt, Opx, Glass
		G		235	Qtz, Pl, Kfs, Bt, Grt, Opx, Glass
A153-A	IH	P	970 ± 10	120	Qtz, Pl, Kfs, Bt, Grt, Opx, Po, Glass
		G		120	Qtz, Pl, (Bt), Ti-Mag, Grt, Opx, Glass
PC2-92-4	PC	P	980 ± 8	237	Qtz, Pl, Bt, Opx, Grt, Glass
PC1-92-20	PC	P	1000 ± 8	288	Qtz, Pl, Opx, Grt, Glass
		G		288	Qtz, Pl, Opx, Grt, Glass
1250 MPa					
PC2-91-11	PC	P	850 ± 8	238	Qtz, Pl, Bt, Grt, Glass
PC2-91-1	PC	P	900 ± 8	168	Qtz, Pl, Bt, Grt, Po, Ap, Glass
PC2-91-4	PC	P	950 ± 8	164	Qtz, Pl, Bt, Opx, Grt, Po, Glass
1500 MPa					
PC2-91-9	PC	P	850 ± 8	264	Qtz, Pl, Bt, Grt, Po, Ap, Glass
PC2-91-14	PC	P	850 ± 8	306	Qtz, Pl, Bt, Grt, Glass
PC2-91-5	PC	P	1000 ± 8	143	Qtz, Pl, Opx, Grt, Glass
1700 MPa					
PC2-91-10	PC	P	850 ± 8	184	Qtz, Pl, Bt, Grt, Glass
PC2-91-8	PC	P	1000 ± 8	97	Qtz, Pl, Opx, Grt, Po, Ap, Rt, Glass
2000 MPa					
PCJRH-91-2	PC	P	850 ± 8	184	Qtz, Pl, Bt, Grt, Glass
PCJRH-92-5	PC	P	900 ± 8	192	Qtz, Pl, Bt, Grt, Rt, Glass
PCJRH-92-4	PC	P	950 ± 8	168	Qtz, Pl, Kfs, Grt, Rt, Glass

pyrrhotite are common accessory phases while apatite was less commonly observed. Phases are homogeneously distributed within the charge if we except a thin magnetite-enriched rim at the contact with the capsule wall in the experiments performed in the internally heated pressure vessel. A description of the main minerals and their *P-T* stability field follows. We first consider the experiments using the mineral powder starting material.

Biotite is a very common phase. It forms small euhedral tablets 5 μm long and 3 μm wide. Its modal abundance decreases both with pressure and temperature. It disappears at high temperature and a biotite-out curve is shown in Fig. 2.

Plagioclase can be observed as euhedral, homogeneous, crystals ranging in size from 3 to 10 μm. Plagioclase is present in all run products except one at 800 MPa and 1026°C.

Quartz is present, in all products, as globular crystals 5 to 10 μm wide, corresponding to sections of very short hexagonal bi-pyramids.

K-feldspar is present is some runs mostly at 1000 MPa. However, this phase is difficult to distinguish from plagioclase and might have been overlooked in some run products. In all cases, we observed a significant increase in the orthoclase content of the residual plagioclase in all run products indicating that K-feldspar is definitely a product of the melting reaction.

Orthopyroxene is an important phase which we expected to appear as a result of the fluid-absent melting of this rock. It appears as elongated crystals 10 to 30 μm long and 3 to 5 μm wide, in the high-temperature portion of the *P-T* diagram. An Opx-in curve is shown in Fig. 2.

Glass is present in all run products except five, as shown in Fig. 2. Three of these came out as powders, a good indication of the absence of melting. Otherwise,

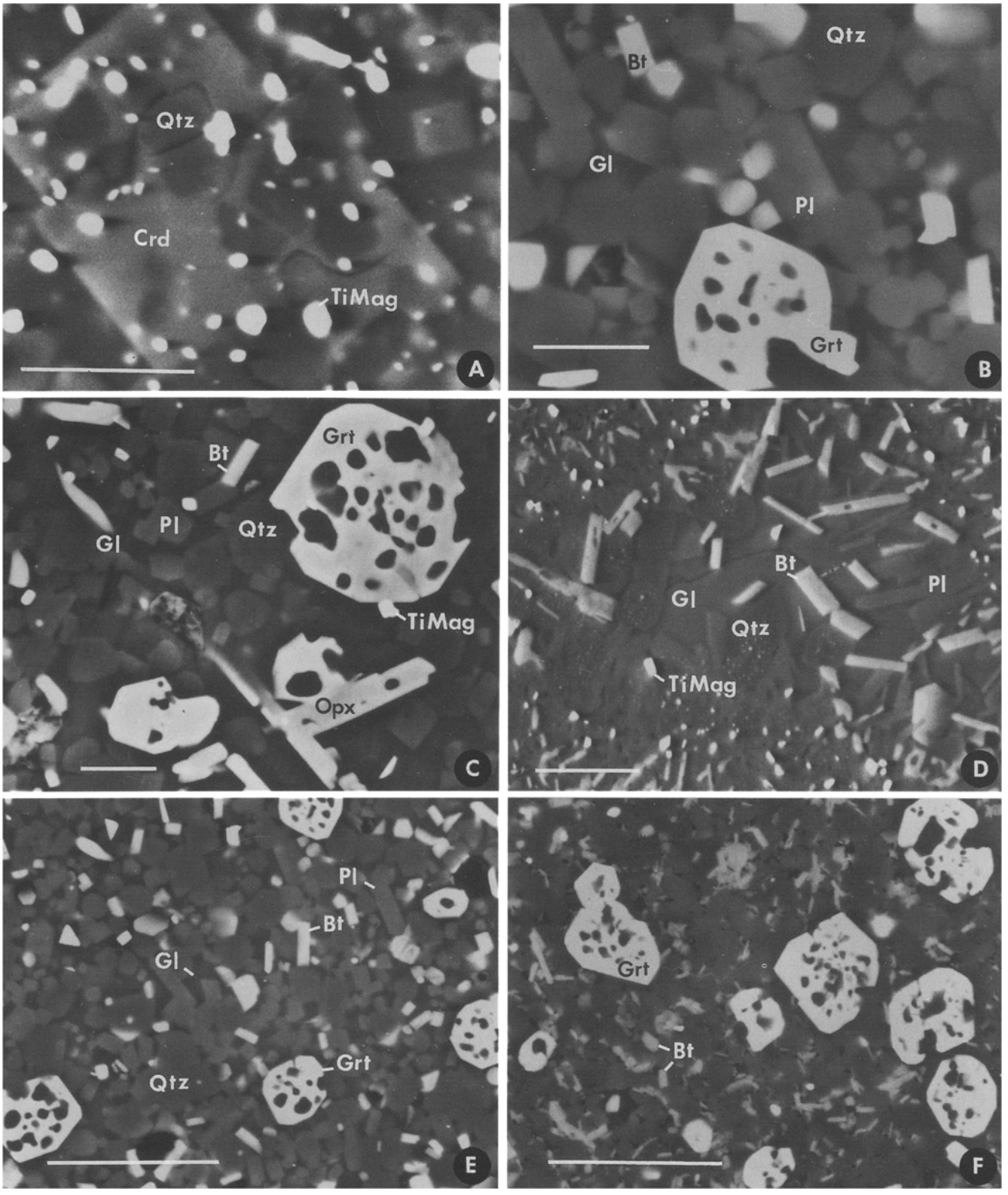

Fig. 1A–F SEM backscattered-electron photographs of some experimental products: **A** Crystal of cordierite with inclusions of quartz and titano-magnetite in experiment CE90-2D (100 MPa, 854°C, 255 h, from powder). **B** Biotite, plagioclase, quartz, garnet and glass in experiment A115C (800 MPa, 875°C, 362 h, from powder). **C** Biotite, plagioclase, quartz, garnet, orthopyroxene, titano-magnetite and glass in experiment A109-A (800 MPa, 886°C, 305 h, from powder). **D** Heterogeneous texture with biotite, plagioclase, quartz, glass, and titano-magnetite in experiment A113-B (1000 MPa, 858°C, 403 h) resulting from the use of glass as a starting material. **E** and **F** Increase of the modal proportion of garnet as a function of pressure: **E** experiment A115-C (800 MPa, 875°C, 362 h, from powder), **F** experiment PC2-91–10 (1700 MPa, 850°C, 184 h, from powder). Quartz and plagioclase cannot be distinguished on this picture. Inclusions in garnet are composed of quartz. The scale bars correspond to 5 μm in photographs **A** to **C** and 20 μm in photographs **D** to **F**

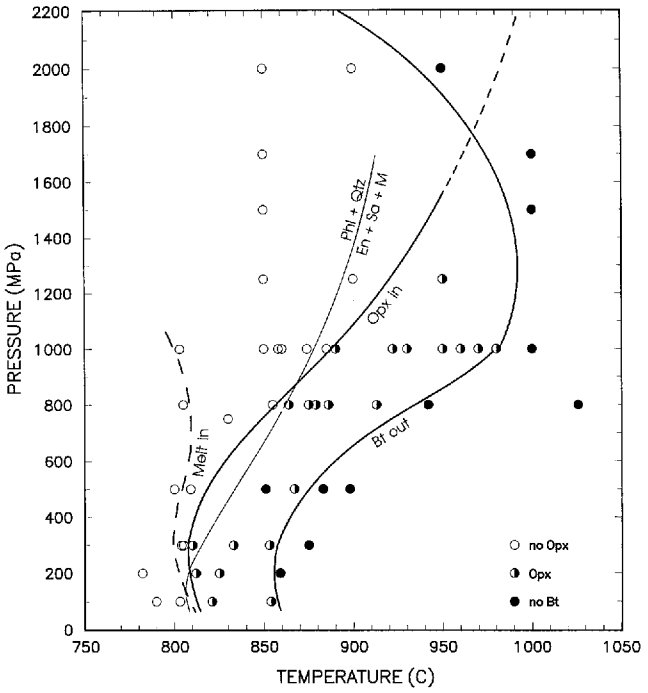

Fig. 2 Pressure - temperature location of some phase boundaries for the CEV-powder (CEVP) composition. The *thin line* corresponds to the reaction Phl + Qtz = En + Sa + M after Vielzeuf and Clemens (1992)

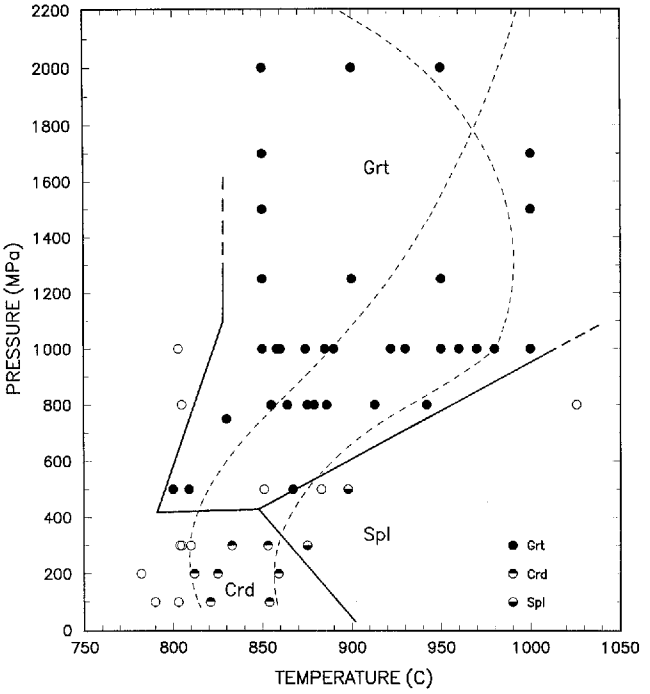

Fig. 3 Pressure - temperature stability fields of garnet, cordierite and spinel for the CEVP starting material. Opx-in and Bt-out *curves* are also shown for a comparison. Note that the Opx and garnet fields do not coincide

the presence of a small amount of glass (< 5 vol.%) is difficult to detect in such experiments. As a result, the location of the solidus shown in Fig. 2 remains uncertain. In all cases, the melt-in and Opx-in curves do not coincide; considering previous petrogenetic modelling, this was unexpected. An explanation will be proposed later.

Cordierite has been observed in seven run products at, and below, 300 MPa (Fig. 3). It develops as large (20 to 30 μm) euhedral crystals containing numerous inclusions of quartz and oxides (Fig. 1). Though commonly associated with orthopyroxene, it has never been observed together with garnet. The stability field of cordierite is shown in Fig. 3.

Garnet is a major phase of interest in this study. It forms rounded crystals about 10 μm wide always showing a characteristic sieve-like texture due to numerous inclusions of quartz (Fig. 1). Its modal proportion increases regularly with pressure; the variation with temperature is more complex and will be discussed later. Garnet is stable over a wide range of P and T as can be seen from Fig. 3. As expected, it is not stable at low pressure where it is replaced by cordierite. At 800 MPa, garnet was no longer present at temperatures over 1000°C.

Spinel is a phase which appeared occasionally at relatively low pressure and high temperature (Fig. 3). It occurs as abundant, very small rounded crystals, usually less than 5 μm in diameter.

Staurolite was found in a single run product at 1000 MPa, 803°C, while *gedrite* was observed in two products at 800 MPa (805 and 855°C).

Oxides: magnetite and/or Ti-magnetite are present in almost all of the runs performed in cold-seal or internally heated vessels. Magnetite forms tiny euhedral crystals. Because of the small size of the crystals, the presence of magnetite or Ti-magnetite may have been missed in some run products. Ilmenite is present in a limited number of runs at and below 800 MPa. In the runs carried out in piston-cylinder vessels, Fe-Ti oxides are absent but pyrrhotite is present as small globules. The difference between piston-cylinder and gas-pressure experiments is ascribed to different f_{O_2} conditions prevailing in the different vessels. However, the high degree of consistency (excluding Fe-Ti oxide stability) between runs carried out in different pressure vessels at the same pressure, suggests that a small change in the f_{O_2} within the vessels is not critical for the major reactions discussed here.

Up to 1000 MPa, most experiments were carried out using both the powder and the glass in separate capsules. The use of glass led to heterogeneous textures in the run products: some pockets composed of a mixture of relatively large crystals (ca 30 μm) and patches of glass are enclosed in a very fine grained (ca 5 μm) groundmass (Fig. 1d). However, no significant difference in mineralogy is observed between the pockets and the groundmass. In the low-temperature runs, a lot of unreacted glass is found and it is even possible to recognize the original particles. The pockets made of large crystals

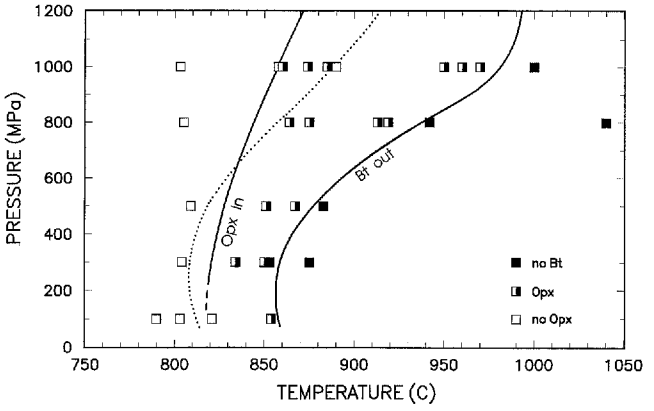

Fig. 4 Pressure - temperature projection of Opx-in and Bt-out *curves* for the CEV-glass composition (CEVG). The *dotted line* corresponds to the Opx-in line from CEVP (Fig. 2). The Bt-out curves are coincident for the two different starting materials

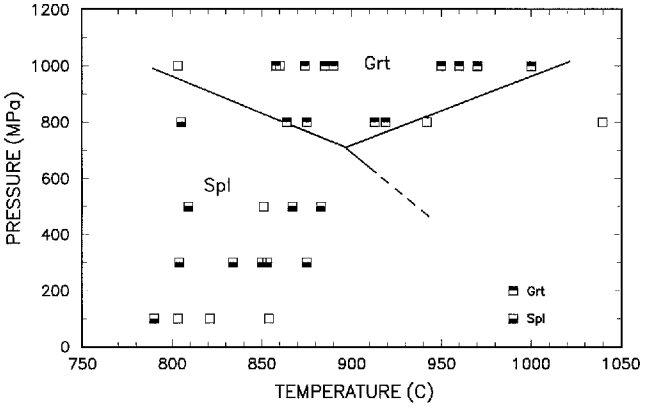

Fig. 5 Pressure - temperature stability fields of garnet and spinel for the CEVG starting material. No cordierite was found in these run products

are preferentially located in the centres of the particles. This heterogeneous character is attributed to a difference in nucleation rates between the cores and rims of the particles. We noticed also a pressure effect on the sizes of crystals; they get bigger as pressure increases. This is true for both starting materials, but the effect is particularly important for the run products from the glass. A consequence is that it is extremely difficult to identify the phases in low-pressure run products, especially below 200 MPa. Some salient features of the mineralogy of the glass experiments are given below:

Biotite does not differ significantly from that in the run products from the powder. It is important to mention that the Bt-out curve shown in Fig. 4 coincides with that determined from the powder.

Orthopyroxene is commonly observed (Fig. 4). Crystals are usually fewer, shorter and fatter than the ones from the powder experiments. An Opx-in curve is shown in Fig. 4 but, although it coincides at low pressure, it differs by about 40°C at 1000 MPa from the Opx-in curve determined from the powder. The Opx appears at a lower temperature in the glass experiments. We believe that the difference can be attributed to metastable growth of orthopyroxene in the glass.

Spinel grew, at and below 800 MPa, as abundant very small (5 μm) crystals. Its stability field, shown in Fig. 5, does not coincide with that determined from the powder (Fig. 3). In particular, no cordierite was observed at low pressure. We believe that spinel grew metastably instead.

Garnet crystallized at 800 and 1000 MPa indifferently in the pockets and the groundmass. They are usually fewer and bigger (up to 30 μm) than in the corresponding powder experiments. Contrary to what we observed in the powder experiments, no garnet was found at 500 MPa.

Metastable mineral growth, and a smaller number of larger crystals are what we would expect from "unseeded" runs on glassy starting materials, where kinetic barriers to nucleation and the unstable nature of the reactants may play a significant role. On the basis of textural (unreacted glass) and mineralogical arguments (extension of the stability fields of orthopyroxene and spinel), we believe that, although complementary, the powder experiments are more reliable than the glass experiments.

Interpretation of the experiments

Melting of biotite + plagioclase + quartz as a function of temperature

The location of the hypothetical fluid-absent reaction

$$\text{Bt}\,(+\,\text{Pl}) + \text{Qtz} = \text{Opx} + \text{Grt/Crd} + \text{Kfs} + \text{melt (M)} \quad \text{(I)}$$

has been discussed earlier by Clemens (1984) and Vielzeuf and Holloway (1988) for average Fe-Mg ratios on the basis of calculations or petrogenetic modelling. In his approach, Clemens (1984) located this curve at about 750–780°C in the range 100 to 1000 MPa while, in the same pressure range, Vielzeuf and Holloway (1988) located reaction (I) at about 850–900°C. First we will check the consistency of this model reaction with our experimental observations then we will discuss its *P-T* location.

As predicted by petrogenetic modelling, the nature of the phase involved in the melting of biotite + plagioclase + quartz changes as a function of pressure. At low pressure, cordierite crystallizes in equilibrium with melt and orthopyroxene. The appearance of cordierite coincides with the appearance of orthopyroxene (except for one run product). Thus, the reaction corresponding to the fluid-absent melting of biotite + plagioclase + quartz below 500 MPa is:

$$\text{Bt} + \text{Pl} + \text{Qtz} \Rightarrow \text{Opx} + \text{Crd}\,(+\,\text{Kfs}) + \text{M} \quad \text{(A)}$$

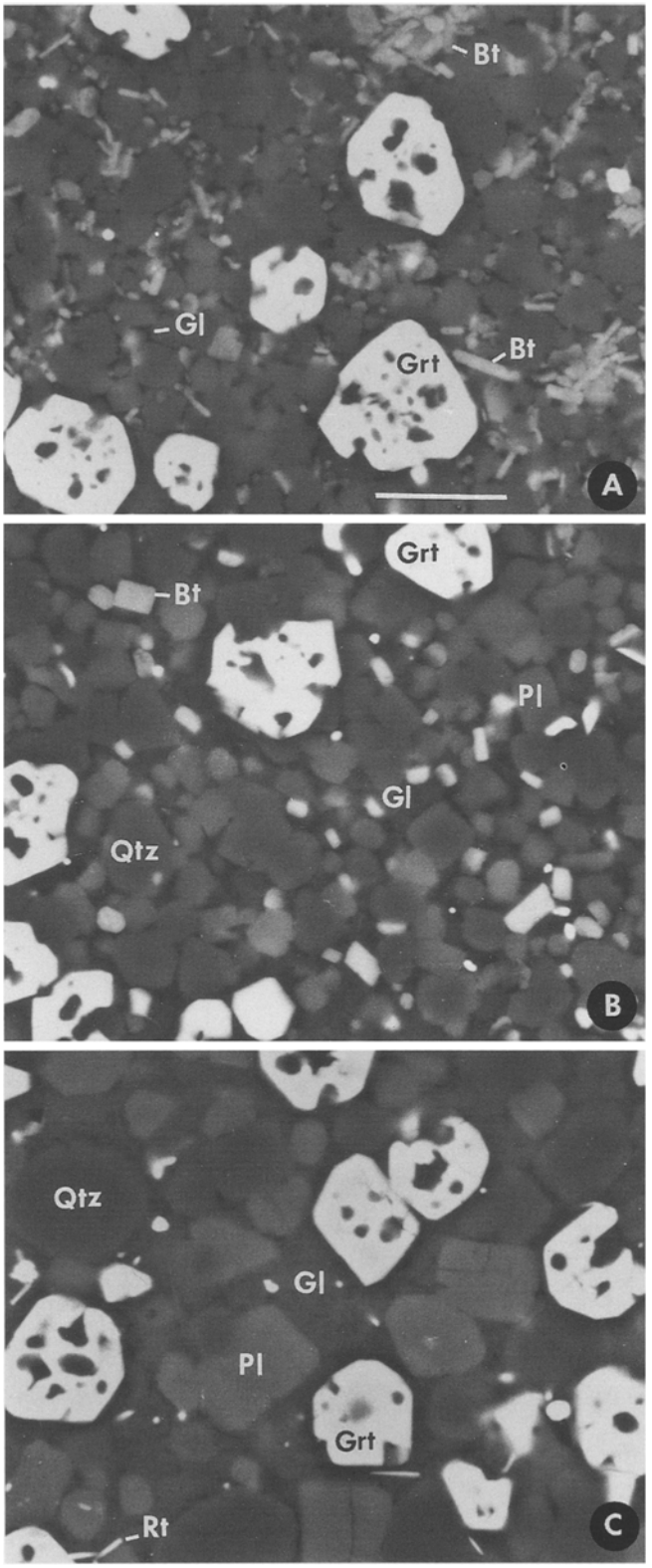

Fig. 6A–C SEM backscattered-electron photographs of 3 experimental products from CEVP at 2000 MPa. **A** 850°C, 184 h, biotite, plagioclase, quartz, garnet, glass. Quartz and plagioclase cannot be distinguished on this picture. **B** 900°C 192 h, biotite, plagioclase, quartz, garnet, glass. **C** 950°C, 168 h, plagioclase, quartz, garnet, rutile, glass. Note the progressive decrease and disappearance of biotite, the increase of the proportion of melt, and the increasing size of the crystals with increasing temperature. Contrary to what happens at lower pressures, no orthopyroxene was produced during the melting process. Inclusions in garnet are composed of quartz. The magnification is the same in the three photographs. The scale *bar* in **A** is 10 μm. Abbreviations as in Table 3

At pressures equal to and greater than 500 MPa, garnet is observed instead of cordierite; thus the reaction is now

$$\text{Bt} + \text{Pl} + \text{Qtz} \Rightarrow \text{Opx} + \text{Grt}\,(+\,\text{Kfs}) + \text{M} \qquad \text{(B)}$$

This reaction has a large pressure extension since it seems valid from 500 MPa up to 1700 MPa.

This ceases to be the case between 1700 and 2000 MPa because, at 2000 MPa, biotite + plagioclase + quartz reacted until disappearance of biotite without producing orthopyroxene (cf. the intersection of the Bt-out and Opx-in curves on Fig. 2). Another important fact is that, contrary to what we would expect from reaction (B) alone, the appearance of garnet does not coincide with the appearance of orthopyroxene (cf. Figs. 2 and 3) and the interval over which garnet is stable in the absence of orthopyroxene increases with pressure. Reaction (B) does not explain these observations and another reaction is required (cf. "Melting of biotite + plagioclase + quartz as a function of P", below).

A complication arises from the crystallization of spinel at high temperature, at 300 and 500 MPa. Because the stability field of both garnet and cordierite is ultimately limited at high temperature, the fluid-absent melting reaction of biotite + plagioclase + quartz in this restricted range of P and T seems to be:

$$\text{Bt} + \text{Pl} + \text{Qtz} \Rightarrow \text{Opx} + \text{Sp}\,(+\,\text{Kfs}) + \text{M} \qquad \text{(C)}$$

In many of our experiments, especially at low pressure, K-feldspar was not observed as a product of the fluid-absent melting of biotite + plagioclase + quartz. However, we observed a strong increase of the orthoclase content in the residual plagioclase (up to 10 mol%) indicating that K-feldspar is definitely "produced" by the melting reaction but does not necessarily crystallize as a separate phase. This is why we indicate Kfs in parentheses in reactions A to D.

Since spinel can be a product of the reaction, we believe that the following:

$$\text{Bt} + \text{Pl} + \text{Qtz} = \text{Opx} + \text{Crd (or Sp or Grt)}\,(+\,\text{Kfs}) + \text{M} \qquad \text{(II)}$$

which is a combination of reactions (A) to (C), is an adequate model reaction for the fluid-absent partial melting of Al-metagreywackes.

We consider that the disappearance of biotite is the indication of the completion of the reaction in the case of a starting material saturated with quartz and plagioclase, provided the kinetics of the reaction are satisfactory. We have already noted that the Bt-out curves using both the powder and the glass coincide, providing

Table 3 List of the reactions quoted in text and Figures

Reaction	Comments
Complex model reactions	
(I) Bt (+ Pl) + Qtz = Opx + Grt or Crd + Kfs + M	Previous models (Thompson 1982; Grant 1985; Vielzeuf and Holloway 1988)
(II) Bt + Pl + Qtz = Opx + Crd (or Spl or Grt) (+ Kfs) + M	This study, a combination of (A), (B) and (C). Kfs present as a separate phase or as a component in plagioclase.
Reactions observed in our experiments	
(A) Bt + Pl + Qtz = Opx + Crd (+ Kfs) + M	*T* dependent
(B) Bt + Pl + Qtz = Opx + Grt (+ Kfs) + M	*T* dependent
(C) Bt + Pl + Qtz = Opx + Spl (+ Kfs) + M	*T* dependent
(D) Bt + Pl + Qtz = Grt (alm-prp-grs) (+ Kfs) + M	*P* dependent
(E) Bt + O_2 = Mag + Kfs + M	f_{O_2} dependent
Reactions involved in Fig. 8	
(1) Phl + Qtz = En + Kfs + Prp + W	
(2) Phl + An = Prp + Grs + Ms	
(3) Prp + Grs + Qtz = En + An	
(4) Grs + Als + Qtz = An	
(5) Ms + Phl + Qtz = Prp + Kfs + W	
(6) Ms + Qtz = Als + Kfs + Phl + W	
(7) Ms + Qtz = Als + Kfs + Prp + W	
(8) Phl + Als + Qtz = Prp + Ms	
(9) Phl + En + An = Prp + Grs + Kfs + W	
(10) Phl + An + Qtz = Prp + Grs + Kfs + W	
(11) Phl + Als + Qtz = Prp + Kfs + W	
Reactions involved in Fig. 9	
(1') Phl + Qtz = En + Kfs + Prp + M	
(2') Phl + An = Prp-Grs + Ms	
(3') Prp-Grs + Qtz = En + An	
(4') Grs + Als + Qtz = An	
(5') Ms + Phl + Qtz = Prp + Kfs + M	
(6') Ms + Qtz = Als + Kfs + Phl + M	
(7') Ms + Qtz = Als + Kfs + Prp + M	
(8') Phl + Als + Qtz = Prp + Ms	
(9') Phl + En + An = Prp-Grs + Kfs + M	
(10') Phl + An + Qtz = Prp-Grs + Kfs + M	
(11') Phl + Als + Qtz = Prp + Kfs + M	
Other reactions used in text	
(12) Qtz + Pl + Kfs + Bt + Crd + Fl = M	
(13) Qtz + Ab + Kfs + Fl = M	

confidence in this result. On the other hand, we believe that the Opx-in curve shown in Fig. 2 represents the beginning of the fluid-absent melting reaction (II). However, the two Opx-in curves from glass and powder experiments, though coinciding at low pressure, differ above 600 MPa (Fig. 4). Thus, we consider that the ending of the melting interval of the fluid-absent reaction (II) has been reversed while the beginning has not.

On these bases, the multivariant projection of the complex reaction (II) onto the *P-T* plane is about 50 to 100°C wide. The reaction shows a significant positive slope, centred at about 835°C at 200 MPa, and 930°C at 1000 MPa. At higher pressures, our experiments are insufficient in number to constrain tightly the location of the reaction. However, it must be located at a *T* lower than 1000°C, at least up to 1700 MPa, because biotite entirely disappeared at these conditions. The results at 2000 MPa are misleading in that they suggest that reaction (B) Bt + Pl + Qtz = Grt + Opx (+ Kfs) + M backbends strongly. This is probably untrue because, although biotite was entirely consumed in the melting process at 2000 MPa and 950°C, no orthopyroxene was found (Fig. 6), suggesting that a melting reaction of another nature than reaction (B) was involved (cf. "Melting of biotite + plagioclase + quartz as a function of *P*").

Our results indicate that reaction (A) backbends towards lower pressure; at 100 MPa, it occurs at a slightly higher temperature than at 200 MPa. The origin of this backbend is uncertain but a similar feature has been observed by Vielzeuf and Clemens (1992) for the fluid-absent melting of phlogopite + quartz. The low-pressure portion of the *P-T* diagram is possibly subject to

complicated phase relationships due to the existence of a thermal barrier and singular points (Grant 1986; Vielzeuf and Clemens 1992).

Melting of biotite + plagioclase + quartz as a function of pressure

The fact that the melt-in and Opx-in curves do not overlap (Fig. 2) indicates that reaction (II) cannot be considered as responsible for the beginning of melting of our starting material. In addition, orthopyroxene was expected to be an essential mineral appearing with garnet and melt (+ Kfs) as a result of the melting of aluminous biotite + quartz (+ plagioclase) according to reaction (B) (Thompson 1982; Grant 1985; Vielzeuf and Holloway 1988). However, it was not anticipated that garnet would appear in the absence of orthopyroxene (compare Figs. 2 and 3). Another point of interest is that, at a given temperature, *the proportion of garnet increases with pressure*, indicating a pressure dependence of the reaction involved. This is illustrated in Figs. 1e and f showing two photographs of run products at 800, and 1700 MPa. In these, garnet coexists with biotite, plagioclase, quartz, and a small amount of melt. The groundmass is composed of small (ca 5 μm) euhedral crystals of quartz and plagioclase, with scattered platelets of biotite. Garnets are larger (ca 10–20 μm) than other crystals and have a characteristic spongy habit.

Though the purpose of this paper is not to discuss the chemical compositions of the coexisting phases, it must be stressed that the grossular content of the garnet is strongly pressure dependent. It increases from about 4 mol% at 500 MPa to about 15 mol% at 2000 MPa.

From these observations, it is clear that biotite, the main Fe-Mg phase in the starting material, breaks down with increasing pressure to a garnet-bearing assemblage. Since garnet incorporates calcium, plagioclase must also participate in the equilibrium. Here again, the orthoclase content of the residual plagioclase increased; therefore Kfs is considered as a product of the reaction in solution in the plagioclase. These mineralogical and compositional changes can be ascribed to another fluid-absent reaction:

$$\text{Bt} + \text{Pl} + \text{Qtz} = \text{Grt (alm-prp-grs)} (+ \text{Kfs}) + \text{M} \quad \text{(D)}$$

with biotite + plagioclase + quartz on the low-pressure side of the reaction.

The crystallization of garnet with increasing pressure critically depends on the composition of the starting material. As a result of solid solutions (s.s.), the bulk composition of our starting material is represented by a mixture of $Bt_I + Pl_I + Qtz$ at low pressure and a mixture of $Bt_{II} + Pl_{II} + Qtz + Grt + M$ at high pressure. The series of experiments at 2000 MPa, clearly shows that biotite may completely react with plagioclase and quartz to produce garnet and melt without producing orthopyroxene. The existence of a reaction such as (D) is an explanation for the intersection of the Bt-out and Opx-in curves between 1500 and 2000 MPa (Fig. 2).

Melting of biotite as a function of f_{O_2}

The initial oxidation state of the biotite is another important variable. The starting material equilibrated under f_{O_2} conditions close to the QFM buffer (Weber and Barbey 1986). Under slightly more oxidizing conditions, such as those in our gas vessels, re-equilibration should occur, according to a reaction such as biotite + $O_2 \Leftrightarrow$ magnetite(Mag) + K-feldspar + H_2O (Eugster and Wones 1962; Skjerlie and Johnston 1994). In quartz-saturated rocks, and above the Qtz + Kfs + H_2O solidus, this reaction becomes

$$\text{Bt} + \text{Qtz} + \text{O}_2 \rightarrow \text{Mag} + \text{Kfs} + \text{M} \quad \text{(E)}$$

Such an "oxidation melting" reaction is a satisfactory explanation for the fact that, at 300 MPa and 805°C, partial melting of biotite occurred without any product other than magnetite and melt.

All the above-mentioned reactions, listed in Table 3, fit the observations and it is possible to match them in a simple petrogenetic model.

Phase relationships

The reaction (II) Bt + Pl + Qtz = Opx + Grt/Spl/Crd + Kfs + M

The results reported in this study are in fairly good agreement with that predicted by the petrogenetic model of Vielzeuf and Holloway (1988), despite the fact that it was constructed for a KFMASH system. Cordierite was expected to be in equilibrium with orthopyroxene, melt and K-feldspar below about 300 MPa while garnet was expected to appear above this pressure. However, differences arise from the relatively rare K-feldspar as a separate phase and the presence of spinel in our experiments.

Spinel, though taken into consideration in the model of Vielzeuf and Holloway (1988), was not expected to interfere with the melting curve of biotite. These experimental results seem to justify some modifications in phase relationships, as shown in Fig. 7. Due to the numerous solid solutions involved in these equilibria (e.g. FeMg-1, NaSiCa-1Al-1, KNa-1 $Al^{IV}Al^{VI}Mg$-1Si-1) leading to complex geometric relationships in the *P-T* projection, an accurate graphic representation is out of the scope of this paper. For clarity, Fig. 7 is constructed for a fixed and average value of *X*Mg of 0.5. The divariant bands for the Fe-Mg reactions are neglected and represented as lines, except for reaction (II) of major interest here. Cordierite is considered as anhydrous. The

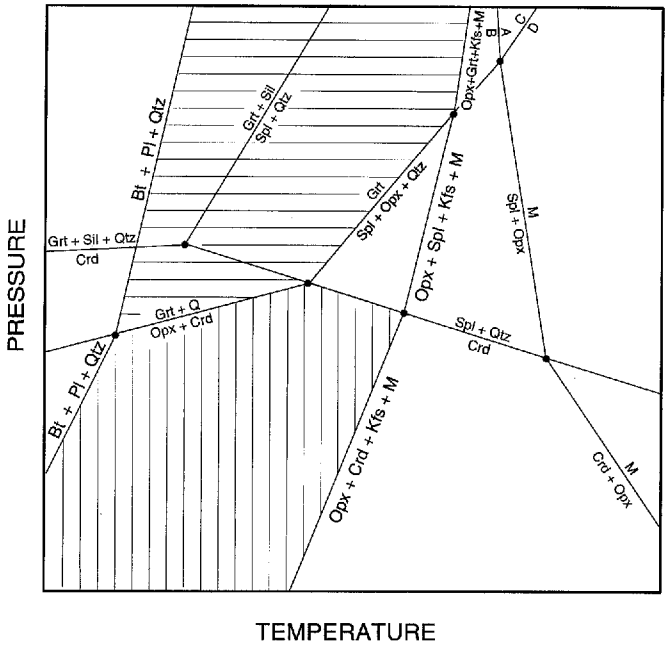

Fig. 7 Hypothetical phase relationships among biotite, plagioclase, quartz (in excess), orthopyroxene, cordierite, spinel, sillimanite and melt in the range 300–500 MPa and 800–900°C. *Vertically striped*, *horizontally striped*, and *shaded areas* correspond to the stability fields of Bt, Pl, Qtz, Opx, Crd, M; Bt, Pl, Qtz, Opx, Grt, M; and Bt, Pl, Qtz, Opx, Spl, M respectively. (*A*: M, *B*: Grt + Opx (+Qtz), *C*: Grt (+Qtz), *D*: Spl + M)

differences between this petrogenetic model and the previous grid (Vielzeuf and Holloway 1988, Fig. 7) arise from the facts that (i) the stability field of spinel + quartz is shifted to lower temperature by about 50°C; (ii) the reactions Crd = Sp + Qtz and Opx + Crd = Grt + Qtz intersect, generating a reaction such as Grt = Sp + Opx + Qtz. The extension of the stability field of spinel + quartz may be the result of a higher f_{O_2}. Additional components such as chromium and zinc will have the same effect (Montel et al. 1986).

Figure 7 also indicates that there should be a reaction such as Grt + Opx (+ Qtz) = M. This could be responsible for the disappearance of garnet at 800 MPa and 1026°C.

Concerning the *P-T* location of reaction (II), the experimental curve is not as steep as predicted. At 200 MPa, biotite disappears at about 850°C while, at 1000 MPa, it disappears between 980 and 1000°C. These data confirm the high thermal stability of biotite in these rocks at high pressure. They complement the experimental work at 1000 MPa of Skjerlie and Johnston (1992) who observed that (i) widespread biotite dehydration melting occurred between 950 and 975°C; (ii) the assemblage Bt + Pl + Qtz was stable up to 1000°C. However they apparently contradict some recent results obtained by G. Stevens and J.D. Clemens (personal communication) and A. Patiño-Douce (personal communication), who found that biotite disappeared at about 930°C at 1000 MPa. An experiment in the gas vessel using our powder (CEVP) and G. Stevens' starting material (GSP) at 1000 MPa and 970°C for 5 days showed no biotite in GSP and a significant amount of biotite in CEVP indicating that slight differences in the composition of the starting material may have a significant effect on the thermal stability of the Bt + Pl + Qtz assemblage.

A comparison between the present results and the location of the Phl + Qtz = En + Sa (sanidine) + M (see Vielzeuf and Clemens 1992, for a review) indicates that:

1. at low pressure, the multivariant field corresponding to the complex melting reaction (II) overlaps the location for the univariant melting of Phl + Qtz;

2. this situation ceases above a pressure of about 800 MPa. There, the melting field of biotite + plagioclase + quartz is located at a higher *T* than the melting curve of Phl + Qtz, and the difference increases with pressure at least up to 1000 MPa (Fig. 2). This indicates that the stabilizing effects of components such as Ti and Ca on the assemblage biotite + plagioclase + quartz are pressure dependent.

According to theoretical phase relations in the KFMASH system, the fluid-absent melting reactions involving muscovite and biotite should produce K-feldspar in equilibrium with a granitic melt (Thompson 1982; Grant 1985; Vielzeuf and Holloway 1988). However, as reported by Patiño Douce and Johnston (1991), K-feldspar has not been reported as a reaction product in many experiments dealing with the fluid-absent melting of micas and excess quartz (Segnit and Kennedy 1961; Patiño Douce and Johnston 1991). Vielzeuf and Holloway (1988) did not report the presence of K-feldspar in their experiments; however in a recent experiment performed at 1000 MPa and 900°C, using the same starting material, we definitely identified K-feldspar as a reaction product. Concerning the fluid-absent melting of phlogopite + quartz, Montana and Brearley (1989) and Peterson and Newton (1989) never reported the presence of K-feldspar while Bohlen et al. (1983) and Vielzeuf and Clemens (1992) did. These last authors reported the scarcity and the difficulty of identifying sanidine in their run products; they noted that the temperature interval over which enstatite, sanidine and melt coexist along the cotectic for the starting material they used was limited because of the chemographic relationships between the coexisting phases. A similar line of argument could be used to explain why K-feldspar was only rarely found in the present experiments. However, there is an alternative explanation:

In the CEV starting material, the proportion of plagioclase is important (32 wt%). This mineral persists after the disappearance of biotite and, as expected from the feldspar ternary diagram (Seck 1971), accomodates a significant amount of orthoclase component (5–10 mol% compared to 1–2 mol% in the starting material). This may prevent the crystallization of K-feldspar as a separate phase until saturation of plagioclase in orthoclase component. No chemical zonation was found in plagioclase indicating that equilibrium was reached

during the experiment. In a series of experiments dealing with the kinetics of the fluid-absent melting of this Al-metagreywacke, Montel (unpublished data) studied the behaviour of a 10–15 mm long, 5 mm diameter, rock cylinder (CEVR) at 500 MPa, 980°C (i.e. 100°C above the disappearance of biotite), for 31 days. Montel observed a mineral assemblage composed of orthopyroxene, spinel, melt, plagioclase, quartz, Fe-Ti oxide, plus abundant K-feldspar as isolated crystals in the melt or as rims around relictual plagioclase. We believe that, due to kinetic problems related to diffusion, dissolution and recrystallization processes, the physical state of the starting material may influence the nature of the phases (especially K-feldspar) in the run product. A very fine powder (less than 5 μm) seems to be a condition to reach equilibrium.

The reaction (D) Bt + Pl + Qtz = Grt + Kfs + M

One of the important steps to construct a petrogenetic model for partial melting of any kind of composition is to determine what are the (metastable) phase relationships among crystalline phases in the absence of melt in the region which will be overlapped by melt. In order to understand the importance of calcium as an additional component, a grid has been constructed for the system SiO_2, Al_2O_3, MgO, CaO, K_2O, H_2O involving the phases quartz, phlogopite, pyrope, grossular, muscovite, aluminium silicate (sillimanite), enstatite, K-feldspar, anorthite, and water (Fig. 8). This was done using the program GeO-Calc (Perkins et al. 1986) and the database of Berman et al. (1985), revised in 1989. Phengitic and eastonitic substitutions in muscovite and phlogopite, respectively, are considered so that phlogopite or pyrope appear on the high-temperature sides of reactions 1, 6, and 7 (cf. Table 3); however the modal proportions of these phases must be low. Figure 8 implies a series of end-member equilibria of primary interest in the understanding of granulite facies metamorphism. Most of them are very familiar to metamorphic petrologists either as pressure dependent (reactions no. 2, 3, 4, and 8) or temperature (and a_{H_2O}) dependent equilibria (no. 1, 5, 6, 7, and 11). On the other hand, the importance of the reaction (10) Phl + An + Qtz = Prp-Grs + Kfs + W (water) has not been recognized widely yet. It is the solid-phase reaction analogue of the melting reaction (D) that we observed in our experiments. The pressure location of reaction (10) is almost independent of the temperature and it should be a good geobarometer (Vielzeuf et al. 1991).

A melt phase (M) has to be taken into consideration because most of the equilibria involved in Fig. 8 lie beyond the solidus represented by the reaction Kfs + An + Qtz + V (vapour) ⇔ M in the KCMASH system. Fig. 9 has been constructed considering that M is, potentially, the most water-rich phase and thus, in a fluid-absent situation, occupies a chemographic location

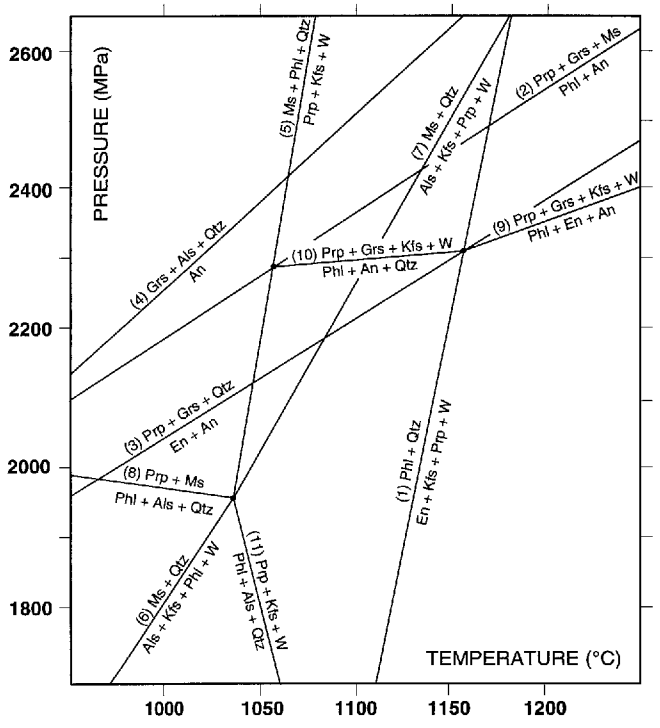

Fig. 8 Calculated end-member *P-T* grid for the system SiO_2, Al_2O_3, MgO, CaO, K_2O, H_2O involving the phases quartz, phlogopite, pyrope, grossular, muscovite, alumino-silicate (sillimanite), enstatite, K-feldspar, anorthite, water

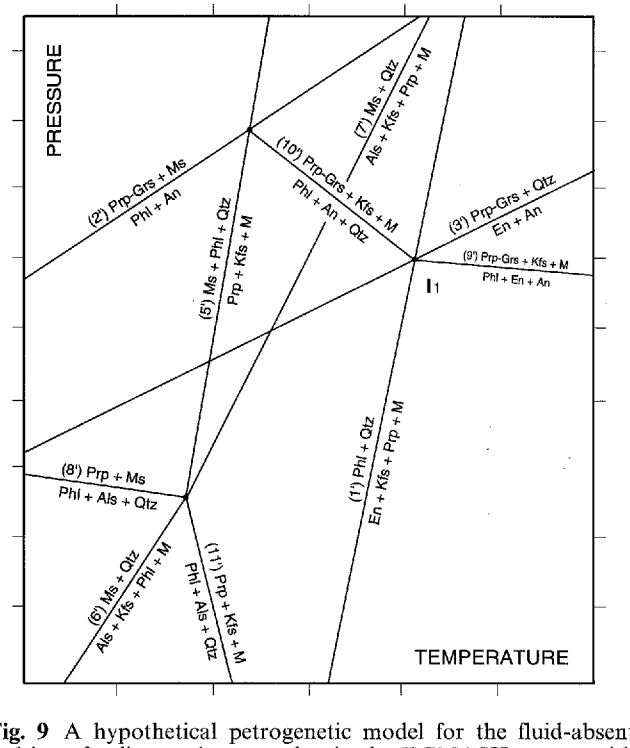

Fig. 9 A hypothetical petrogenetic model for the fluid-absent melting of pelites and greywackes in the KCMASH system with emphasis on the assemblages involving an anorthite component in the plagioclase. Scales on *P* and *T* axes are schematic and do not correspond to those in Fig. 8

analogous to W. In addition, the slightly positive slope of reaction 10 has been changed arbitrarily to slightly negative (10') in order to locate the melt phase on the high-temperature side of the reaction. The strongly negative slope of reaction 11' could be modified to strongly positive without modifying our conclusions. In this figure, some end-members of the most important reactions involved in the partial melting of crustal lithologies are represented (e.g. 1', 6', 7', 11'). The purpose of this figure is to highlight some other important but commonly overlooked equilibria involving anorthite and grossular components such as 10' Phl + An + Qtz ⇔ Grt (prp-grs) + Kfs + M. Reactions involved in Fig. 9 are listed in Table 3.

In order to understand processes in complex systems, multivariant fields should be taken into consideration. Due to the difficulty to represent graphically in a rigorous manner the multivariant fields involving several complex substitutions, no attempt will be made here. However, it is worth noting that most of the equilibria involving only Fe-Mg substitution in this diagram have rather narrow divariant fields, for a given composition [e.g. reactions 1' and 11' with the notable exception of reaction 8' (see Holdaway 1980; Vielzeuf 1984; Berman 1990)]. On the other hand, for a given bulk composition, all of the equilibria involving anorthite have very wide, pressure dependent, multivariant fields, which makes them particularly suitable as geobarometers. This is the case for reaction 10', as shown by our experiments.

With increasing pressure and in the range 800–850°C, biotite, the anorthite component in the plagioclase and quartz progressively reacted to give $garnet_{s.s.}$ + $K\text{-feldspar}_{in\ plag}$ + melt. At lower temperatures, muscovite (Ms) is expected to appear in a bulk composition such as the one we used in these experiments. Indeed, muscovite is a common phase in amphibolite facies metagreywackes. Thus the fluid-absent melting of these rocks should first occur in connexion with reactions (6') Ms + Qtz = Kfs + Als (aluminium-silicate) + Bt + M or (5') Ms + Bt + Qtz = Grt (alm-prp) + Kfs + M. However, too few experiments were done in this area to constrain the reactions responsible for the beginning of melting. Furthermore, other phases such as staurolite and gedrite may complicate the scenario.

The fact that the assemblage biotite + plagioclase + quartz progressively breaks down with increasing pressure, with the ability to generate a melt, provides an explanation for the apparent disagreement between the experimental results of Vielzeuf and Holloway (1988) and Le Breton and Thompson (1988). This concerns the location of the reaction Bt + Sil + Pl + Qtz = Grt + Kfs + M at 1000 MPa. The first authors consider that, at 1000 MPa, this reaction has a narrow multivariant field ("probably less than 20°C") located at about 850°C ± 15°C. On the other hand, at the same pressure, Le Breton and Thompson observed that melting began between 760 and 800°C and was extensive at 850°C (with biotite still present). Consequently, they located the reaction some 70°C below the location proposed by Vielzeuf and Holloway. The fact that Le Breton and Thompson observed melting at a temperature less than 800°C could be tentatively ascribed to the fact that some biotite + plagioclase + quartz, originally equilibrated at about 700–800 MPa, may have reacted at 1000 MPa to give some melt. In this case, as in the present study, the first appearance of melt could coincide with the melting reaction 6' and not 11'. Indeed, the width of the multivariant field of the reaction Bt + Sil + Pl + Qtz = Grt + Kfs + M is rather difficult to document. This is because, although it is easy to determine where the multivariant field ends by observing the disappearance of biotite (~ 860°C), it is very difficult to determine where it begins in the absence of crystallization of a new phase such as orthopyroxene in the present study.

In conclusion: (1) in most cases, above 500 MPa, the beginning of the fluid-absent melting of both Ca-poor Al-metagreywackes and metapelites corresponds to melting reactions involving muscovite; (2) the pressure-dependent reaction Bt + $An_{(component\ in\ plag)}$ + Qtz ⇔ Grt_{ss} + $Kfs_{in\ Plag}$ + M is fundamental for the understanding of the evolution of phase relationships in these rocks in the range 800–900°C, 500–2000 MPa; (3) in Ca-poor Al-metagreywackes, extensive melting occurs in response to the reaction Bt + Pl + Qtz ⇔ Opx + Crd/Spl/Grt + Kfs + M.

More on the multivariant field of Bt + Pl + Qtz + Opx + Grt + Kfs + M

We have demonstrated experimentally that there is a ~ 50 to 100°C wide interval over which biotite, quartz, plagioclase, orthopyroxene, garnet and melt coexist. This field does not correspond to a simple divariant field of a single reaction, such as 1', but rather to the superposition of the multivariant fields of four different reactions. Indeed, in the pure, theoretical Mg system, these phases coexist at I_1 on Fig. 9. The various univariant curves that intersect at I_1 are:

(1') Phl + Qtz → En + Kfs + Prp + M (increasing *T*)

(3') En + An → Prp-Grs + Qtz (increasing *P*)

(10') Phl + An + Qtz → Prp-Grs + Kfs + M (increasing *P*)

(9') Phl + En + An → Prp-Grs + Kfs + M (increasing *P*).

If we take the various solid solutions into consideration and if we replace Phl, En, Prp-Grs by Bt, Opx, Grt respectively, I_1 becomes a *P-T* surface which has been schematized in Fig. 10. In addition, we consider that the multivariant field of reaction (1') (the An-absent reaction) is small compared to the others. These reactions and their multivariant fields are helpful in predicting the modal changes that will occur within this multivariant

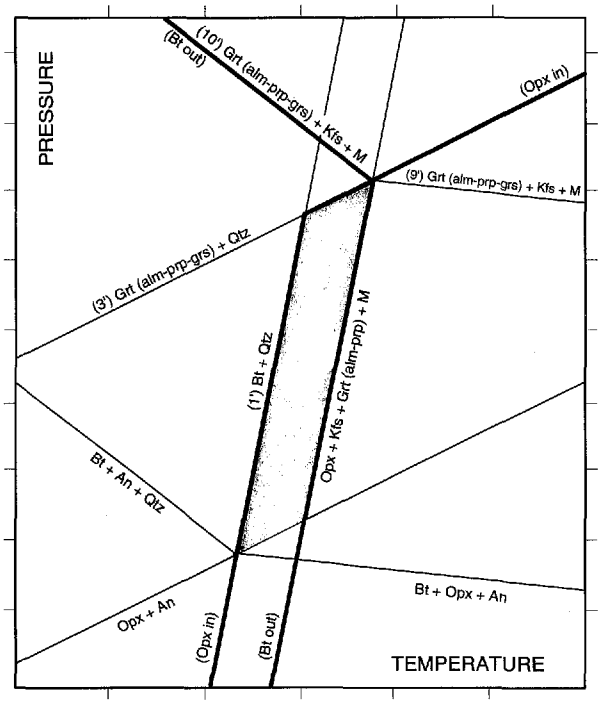

Fig. 10 A petrogenetic interpretation of the multivariant field within which biotite, quartz, plagioclase, orthopyroxene, garnet and melt coexist

Table 4 Prediction of the modal changes of the phases within the multivariant field defined by the co-stability of biotite - plagioclase - quartz - garnet - orthopyroxene - melt (figure 10), as a function of increasing pressure (constant *T*) or temperature (constant *P*). The modal proportion of the phase increases (*inc*) or decreases (*dec*)

	Increasing *P*	Increasing *T*
Bt	Dec	Dec
Qtz	?	Dec
Pl (An)	Dec	Inc
Pl (Ab)	Dec	Dec
Kfs	Inc	Inc
Opx	Dec	Inc
Grt (alm-prp)	Inc	Inc
Grt (grs)	Inc	Dec
M	Dec	Inc

domain (Table 4). Biotite and quartz should decrease with increasing temperature while orthopyroxene, garnet (alm-prp), Kfs and melt should increase. With increasing pressure, biotite, orthopyroxene, and the anorthite component in the plagioclase should decrease while the modal proportion of garnet (alm-prp-grs), and K-feldspar should increase. Orthopyroxene-in and Bt-out curves have been drawn on Fig. 10 for a starting material composed of Bt + An + Qtz (with excess Qtz and An with respect to Bt); they intersect at high pressure. From this figure, it appears that the Bt-out curve is a composite of two different reactions (Bt + Qtz = Opx + Kfs + Grt (alm-prp) + M and Bt + An + Qtz = Grt (alm-prp-grs) + Kfs + M); the same applies for the Opx-in curve (Bt + Qtz = Opx + Kfs + Grt (alm-prp) + M and Grt (alm-prp-grs) + Qtz = Opx + An). This is a possible interpretation for the intersection of the Bt-out and Opx-in curves in Fig. 2.

The schematic *P-T* diagram shown in Fig. 10 represents a satisfactory explanation of our experimental observations in the range 500–2000 MPa. At low pressures, these relationships are no longer valid because of the influence of other phases, such as cordierite and spinel.

In this discussion, the albite component of the plagioclase has not been taken into account. Since melt is the only other phase that can incorporate sodium in this *P-T* range, the albite component in the plagioclase should decrease as the melt proportion increases. As we can see on Fig. 10, pressure will have a similar effect on both the albite and anorthite components and we can conclude that the modal proportion of plagioclase should decrease with increasing *P*.

Fig. 10 is inadequate to predict the evolution of the proportion of melt with pressure, since this is strongly dependent on the solubility of water in the melt. However, since this solubility increases strongly with pressure, we expect the proportion of melt to decrease concomitantly, at constant *T* (Clemens and Vielzeuf 1987).

We believe that the method of "decomposing" the complex equilibria into simpler end-member reactions is a necessary step in understanding partial melting processes involving solid solutions.

Modelling the proportion of melt

As previously discussed by various authors (Robertson and Wyllie 1971; Eggler 1973), in a *P-T* projection of an hypothetical A-H_2O system involving an anhydrous crystalline phase (A), a hydrous phase (H), a hydrous melt (M), and a fluid phase (Fl) (Clemens and Vielzeuf 1987, Fig. 1), all but the Fl-absent reactions will shift in response to lowered activity of water. The locus of the fluid-absent melting reaction (Fl) is thus coincident in *P* and *T* with the intersections of the solidus (H or A + Fl = M) and the sub-solidus dehydration (H = A + Fl) curves, for various a_{H_2O} in the melt or in the fluid phase. This spatial coincidence is only valid if the diluting species used to lower a_{H_2O} in the fluid phase (e.g. CO_2) is perfectly insoluble in the melt, a strictly incorrect, but useful assumption (Eggler 1973; Eggler and Holloway 1977). From simple geometrical considerations, as illustrated in Fig. 11, the intersections of these two sets of curves can give rise to a reversal of dP/dT slope for the fluid-absent curve, negative at low pressure, positive at high pressure. This could be an explanation for the negative slope we observed at low pressure for both reactions: Phl + Qtz = En + Sa + M (Vielzeuf and Clemens 1992) and Bt + Pl + Qtz = Opx + Crd + Kfs + M (this study).

The activity of water and the water contents in the melt change along the fluid-absent curve, and are

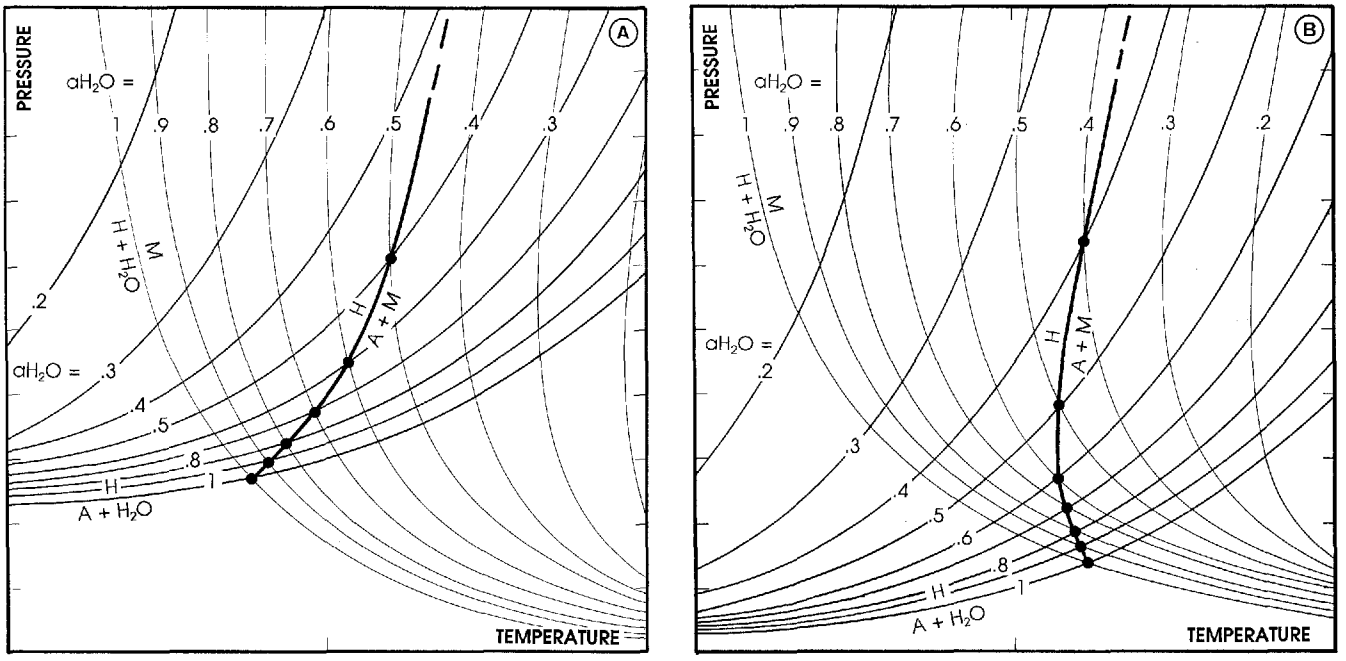

Fig. 11A,B Geometrical relationships between solidus and sub-solidus reactions calculated for various activities of water in the fluid phase. The intersections of the two sets may generate an inversion of the slope of the fluid-absent reaction (**B**). See text for explanation. (*H* hydous crystalline phase, *A* anhydrous crystalline phase, *M* hydrous melt

uniquely defined at P and T. In the system we studied, the locus of the fluid-absent melting reaction (II) can be approximated as the intersection of the solidus (Qtz + Pl + Kfs + Bt + Crd + Fl = M) and the sub-solidus (Bt + Pl + Qtz = Opx + Crd + Kfs + Fl) curves, for various a_{H_2O}. Experimental data (Whitney 1975; Johannes 1984) show that a small addition of components such as excess Al, Ca, Mg or Fe do not significantly change the location of the haplogranite solidus. Thus, reaction (12) Qtz + Pl + Kfs + Bt + Crd + Fl ⇔ M must be close to reaction (13) Qtz + Ab + Kfs + Fl ⇔ M which can be considered as an excellent thermodynamic analogue of reaction (12). A computer programme, written by Nekvasil and Burnham (1987), allows the calculation of the P-T location of reaction (13) as a function of a_{H_2O} (Fig. 12). Ebadi and Johannes (1991) experimentally determined the P-T locations of these curves by diluting the fluid phase with CO_2. In the P-T range of interest, the agreement between the two sets of curves is good. The intersections of these with the fluid absent field determined in this study allows approximate determination and qualitative evolution of a_{H_2O} along the multivariant fluid-absent reaction Bt + Pl + Qtz = Opx + Crd (or Grt) + Kfs + M. According to these data, the a_{H_2O} in the melt decreases rapidly from 1 to 0.4 ± 0.1 between 50 MPa and 200 MPa. It decreases slowly from 0.4 ± 0.1 to 0.15 ± 0.05 between 200 and 1000 MPa, and it increases slightly to about 0.3 above 1000 MPa. Errors are quoted to take into account the width of the multivariant field but cannot

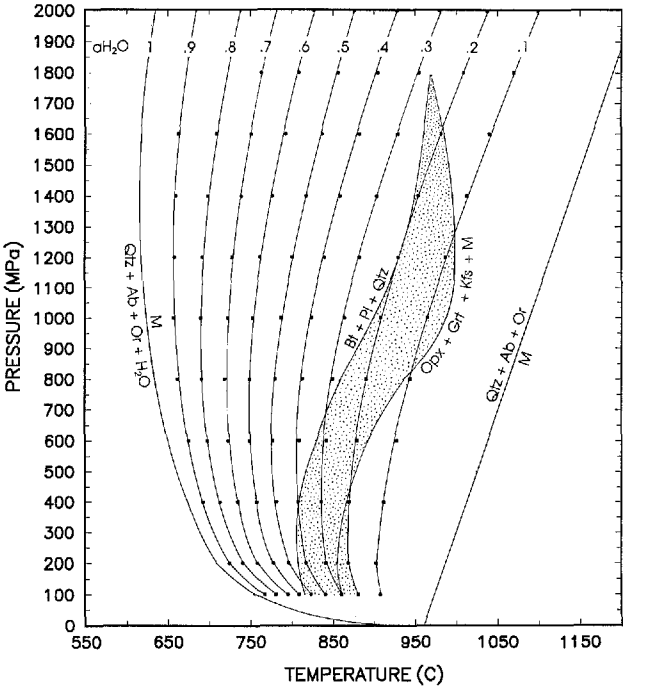

Fig. 12 P-T diagram showing the locus of reaction Ab + Sa + Qtz + H_2O ⇔ M (*thin solid lines*) as a function of a_{H_2O}, as calculated using the computer programme of Nekvasil and Burnham (1987), based on a model for alumino-silicate melt-water interactions (Burnham 1979 ; Burnham and Nekvasil 1986). The intersections of these curves with the fluid-absent reaction Bt + Pl + Qtz = Opx + Crd/Spl/Grt + Kfs + M determined experimentally provide rough estimates of the a_{H_2O} in the melt in our experiments

account for any errors in the calculation procedure of the model. The values of a_{H_2O} determined using the curves of Ebadi and Johannes (1991) are within these error bars.

The same programme (Nekvasil and Burnham 1987; Nekvasil 1988) allows the calculation of the isopleths of constant X_{H_2O} or wt% H_2O in the melt. These can be used to determine the amount of water in the melt at P and T along the fluid-absent curve (Clemens and Vielzeuf 1987; Vielzeuf and Clemens 1992). Figure 13 shows that the water content of the melt increases from 2 ± 0.5 to 3 ± 0.5 wt% between 100 and 200 MPa, stays almost constant (3 ± 0.5 wt%) between 200 and 1000 MPa, and then increases significantly above this pressure. The starting material is such that biotite is the first phase to disappear. Thus, we assume that water is the limiting factor for melting, in other words, that the amount of melt at P and T is a simple function of the amount of water in the starting material. At the temperature where biotite completely disappears, the amount of melt can be calculated using the relation: *wt% H_2O in the starting material* · 100/ wt% H_2O in the melt (Clemens and Vielzeuf 1987). According to this relation, the amount of melt observed when the biotite completely disappears should rapidly decrease from $\sim 70 \pm 5$ to 60 ± 5 wt% between 100 and 200 MPa, remain almost constant ($\sim 60 \pm 5$ wt%) between 200 and 1200 MPa and progressively decrease to about 25 wt% at 1800 MPa. Small errors in the model or the location of the fluid-absent curve may lead to large errors in the determination of both the activity of water along the melting curve and the proportion of melt. However, this model remains useful for predicting the qualitative evolution of the proportion of melt with increasing pressure. In a subsequent paper (J.M. Montel and D. Vielzeuf, in preparation), we will discuss how these estimates compare with mass balance calculations and image processing results.

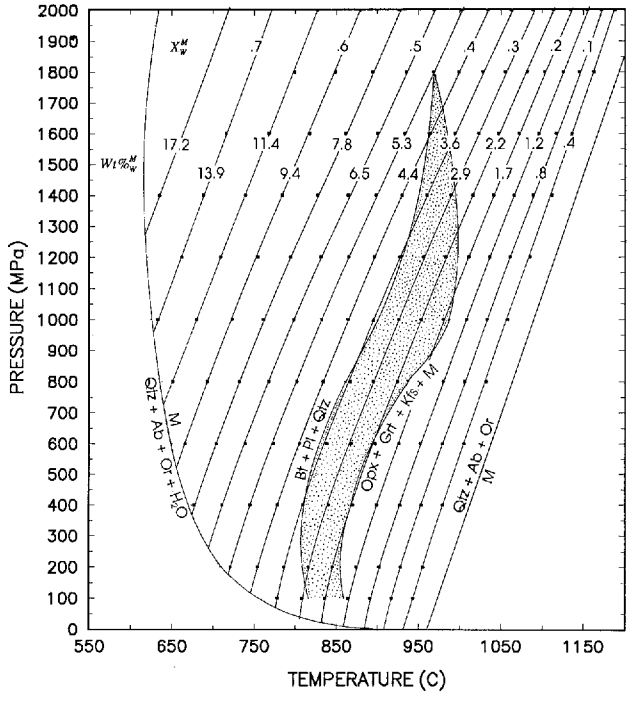

Fig. 13 Isopleths of constant X_{H_2O} in the melt (X_W^M) (corresponding to almost constant wt% water in the melt) calculated using the computer program of Nekvasil and Burnham (1987). Labels for the intermediate values of X_W^M (0.05, 0.15, 0.25 ...) are not shown for clarity. The intersections of these *curves* with the fluid-absent reaction Bt + Pl + Qtz = Opx + Crd/Spl/Grt + Kfs + M provide estimates of the water content of the melt (and thus its modal proportion) at P and T in our experiments

Conclusion: implications for the P-T formation of granulites

The most important reaction involved in the partial melting of Al-metagreywackes is (II) Bt + Pl + Qtz = Opx + Crd/Spl/Grt + Kfs + M. Its multivariant field is ~ 50 to 100°C wide. The experimental curve is much less steep than usually considered: at 200 MPa, biotite disappears at about 850°C while it disappears between 980 and 1000°C at 1000 MPa, pointing out the high thermal stability of biotite + plagioclase + quartz at high-pressure. This is an explanation for the field observation that orthopyroxene is relatively rare in high pressure quartzo-feldspathic granulites while this mineral is characteristic of medium- to low-pressure quartzo-feldspathic granulites throughout the world. This is nicely exemplified by reference HP-HT rocks from the Hercynian belt of Europe (see Pin and Vielzeuf 1983, for a review).

This study shows that Ca-poor Al-metagreywackes represent fertile rocks at commonly attainable crustal temperatures, below 700 MPa. There, we anticipate that 30 to 60% of melt can be produced. Above this pressure, temperatures above 900°C are required, making the production of granitoid magmas more difficult.

Above 300 MPa, orthopyroxene, garnet, plagioclase, and quartz can be in equilibrium with a granitoid melt as already shown by Clemens and Wall (1981), Conrad et al. (1988), Vielzeuf et al. (1990); Skjerlie and Johnston (1993). Interestingly, thin layers of gneisses composed of orthopyroxene, garnet, plagioclase, and quartz ± biotite and interbedded within sillimanite bearing paragneisses are quite common within granulite terrains throughout the world. The idea that they may result from partial melting of metagreywackes is appealing. They could correspond to a recrystallized mixture of crystals (+ trapped melt) left behind after removal of a major proportion of melt (+ small fraction of entrained crystals). This is commonly considered as an hypothesis for the origin of some granulites (Clemens and Wall 1981; Waters 1988; Conrad et al. 1988; Vielzeuf and Holloway 1988; Patiño Douce and Johnston 1991). If this hypothesis is accepted, the P-T surface corresponding to the reaction Bt + Pl + Qtz = Opx + Crd/Spl/Grt + Kfs + M, as shown in Fig. 2, provides important temperature constraints on the metamorphism.

The experimental constraints on the partial melting of pelites are rather limited in pressure; most of the data were collected at 1000 MPa. However, these are sufficient to demonstrate that the partial melting of pelites takes place at a lower temperature (850°C ± 20) than the melting of Al-metagreywackes (930°C ± 40). The *P-T* domain between 900°C ± 50 at 1000 MPa and 800°C ± 50 at 200 MPa represents the region where most common crustal metasediments (pelites and Al-greywackes) can melt under fluid-absent conditions. Because melting reactions are efficient thermal buffers (see Vielzeuf et al. 1990 for a review), the maximum temperature reached during granulite facies metamorphism will be controlled by melting processes in same cases.

The common observation that biotite is no longer stable in aluminous paragneisses while it still coexists commonly with orthopyroxene, garnet, plagioclase and quartz, provides rather tight constraints on the prograde maximum *T*. It indicates: (i) that the temperature of metamorphism exceeded the temperature of melting of the metapelites; (ii) that the melting of metagreywackes did not go to completion. The contrasting melting behaviour of the two sets of rocks is thus another useful indicator of temperatures reached during metamorphism. This semi-quantitative method of determining metamorphic conditions provides temperatures usually higher, by about 100°C, than those recorded by the most common geothermometers (Vielzeuf, unpublished data on granulites from the Pyrenees or the Ivrea Zone in the Alps).

Another conclusion is that, at temperatures below reaction (II), biotite + plagioclase + quartz progressively react, with increasing pressure, to give garnet + $Kfs_{in\ pl}$ + melt (reaction D). The multivariant field of this reaction is huge and can be used as a geobarometer provided independent estimates of a_{H_2O} can be made (Vielzeuf et al. 1991). It shows that pressure may play a complementary role to temperature for the breakdown of hydrous minerals and melting in the crust. The progressive replacement of biotite by garnet with increasing grade of metamorphism is documented in many field areas. One of the best examples is in the Ivrea Zone, with the progressive transition from biotite – sillimanite gneisses to garnet – sillimanite "stronalites" (Schmid and Wood 1976). Such features are commonly ascribed to an increase in temperature and reactions such as Bt + Pl + Sil + Qtz = Grt + Kfs + M. However, it can be observed that pressure will have a similar effect: increasing the modal proportion of garnet at the expense of biotite. Although not as drastic as temperature, the pressure effect on the appearance, or disappearance, of biotite may be of some importance in some particular cases: in the southern part of Armorican Massif, a part of the Hercynian belt of France, Lasnier et al. (1973) described reactional textures made of garnet and K-feldspar at the contact between biotite and plagioclase in an orthogneiss. This texture has been ascribed to the reaction Bt + Pl + Qtz → Grt + Kfs + H_2O (reaction 10) which is the sub-solidus analogue of reaction (D). This reaction has been interpreted as the result of the prograde transformation of a granite undergoing high-pressure metamorphism. Similar textures have been described by Griffin and Heier (1969) in the high-pressure granulites from Norway. Conversely, a decrease in pressure could have played later an important role in retrograde re-hydration and crystallization of extensive biotite in these high-pressure granulites.

Abbreviations

(used in text, tables and figures:)

Ab albite; *alm* almandine component in garnet; *Als* aluminum silicate; *An* anorthite; *Ap* apatite; *Bt* biotite; *Cal* calcite; *Crd* cordierite; *Crn* corundum; *En* enstatite; *Fl* fluid phase; *Fs* ferrosilite; *Ged* gedrite; *Gl* glass; *Grs* Grossular; *grs* grossular component in garnet; *Grt* garnet; *Hc* hercynite; *Hem* hematite; *Ilm* ilmenite; *Kfs* K-feldspar; *M* melt; *Mag* magnetite; *Ms* muscovite; *Opx* orthopyroxene; *Or* orthoclase; *Phl* phlogopite; *Pl* plagioclase; *Po* Pyrrhotite; *Prp* pyrope; *prp* pyrope component in garnet; *Qtz* quartz; *Rt* rutile; *Sa* sanidine; *Sil* sillimanite; *Spl* spinel; *St* staurolite; *Ti-Mag* titano-magnetite; *W* water.

Acknowledgements This study has been supported by CNRS-INSU through contracts 91 DBT 3.28 and 91 DBT 4.09. The final stage of the programme benefited from a NATO collaborative research grant to D.V.. The 2000 MPa piston-cylinder experiments were done by D.V. during a stay in J.R. Holloway's laboratory at Arizona State University. We are grateful to J.R. Holloway for his financial support and to A. Pawley, Y. Thibault and R.A. Brooker for their help and discussions. Some experiments in the range 1000–1700 MPa were performed in collaboration with R. Kryza who visited Clermont for 6 months. He is gratefully acknowledged for his assistance and for letting us use some unpublished data. D. Laporte, M. Schmidt, A. Patiño Douce, G. Stevens, J.D. Clemens, J.A. Grant, and D.J. Waters provided reviews of the successive manuscripts, which helped us in clarifying our views and interpretations. This is contribution CNRS-INSU-DBT no. 682, thème "Fluides, Minéraux et Cinétique".

References

Berman RG (1990) Mixing properties of Ca-Mg-Fe-Mn garnets. Am Mineral 75:328–344

Berman RG, Brown TH, Greenwood HJ (1985) An internally consistent thermodynamic data base for minerals in the system Na_2O - K_2O - CaO - MgO - FeO - Fe_2O_3 - Al_2O_3 -SiO_2 - TiO_2 - H_2O - CO_2. Atomic Energy of Canada Ltd Technical Report 377

Bohlen SR, Boettcher AL, Wall VJ, Clemens JD (1983) Stability of phlogopite-quartz and sanidine-quartz: a model for melting in the lower crust. Contrib Mineral Petrol 83:270–277

Chappell BW (1984) Source rocks of I- and S-type granites in the Lachlan Fold Belt, Southeastern Australia. Philos Trans R Soc London A310:693–707

Clemens JD (1984) Water contents of intermediate to silicic magmas. Lithos 11:213–287

Clemens JD, Vielzeuf D (1987) Constraints on melting and magma production in the crust. Earth Planet Sci Lett 86:287–306

Clemens JD, Wall VJ (1981) Crystallization and origin of some peraluminous (S-type) granitic magmas. Can Mineral 19:111–132

Clemens JD, Wall VJ (1984) Origin and evolution of a peraluminous silicic ignimbrite suite: the Violet Town Volcanics. Contrib Mineral Petrol 88:354–371

Conrad WK, Nicholls IA, Wall VJ (1988) Water-saturated and undersaturated melting of metaluminous and peraluminous crustal compositions at 10 kbar: evidence for the origin of silicic magmas in the Taupo Volcanic Zone, New Zealand, and other occurrences. J Petrol 29:765–803

Ebadi A, Johannes W (1991) Beginning of melting and composition of first melts in the system Qz - Ab - Or -H_2O - CO_2. Contrib Mineral Petrol 106:286–295

Eggler DH (1973) Principles of melting of hydrous phases in silicate melt. Carnegie Inst Washington Yearb 72:491–495

Eggler DH, Holloway JR (1977) Partial Melting of peridotite in the presence of H_2O and CO_2 : principles and review. Magma genesis, Oregon Dept Geol Min Ind Bull 96:15–36

Eugster JP, Wones DR (1962) Stability relations of the ferruginous biotite, annite. J Petrol 3:82–125

Grant JA (1985) Phase equilibria in partial melting of pelitic rocks. In: Ashworth JR (ed) Migmatites. Glasgow, Blackie and Son, pp 86–144

Grant JA (1986) Quartz-phlogopite-liquid equilibria and origins of charnockites. Am Mineral 71:1071–1075

Griffin WL, Heier KS (1969) Parageneses of garnet in granulite-facies rocks, Lofoten-Vesteraalen, Norway. Contrib Mineral Petrol 23:89–116

Hoffer E, Grant JA (1980) Experimental investigation of the formation of cordierite-orthopyroxene parageneses in pelitic rocks. Contrib Mineral Petrol 73:15–22

Holdaway MJ (1980) Chemical formulae and activity models for biotite, muscovite and chlorite applicable to pelitic metamorphic rocks. Am Mineral 65:711–719

Hoschek G (1976) Melting relations of biotite + plagioclase + quartz. Neues Jahrb Mineral Monatsh 2:79–83

Johannes W (1984) Beginning of melting in the granite system Qz - Or - Ab - An - H_2O. Contrib Mineral Petrol 86:264–273

Lasnier B, Leyreloup A, Marchand J (1973) Découverte d'un granite "charnockitique" au sein de "gneiss oeillés": perspectives nouvelles sur l'origine de certaines leptynites du Massif Armoricain méridional (France). Contrib Mineral Petrol 41:131–144

Le Breton N, Thompson AB (1988) Fluid-absent (dehydration) melting of biotite in metapelites in the early stage of crustal anatexis. Contrib Mineral Petrol 99:226–237

Marignac C, Leroy J, Macaudiere J, Pichavant M, Weisbrod A (1980) Evolution tectonométamorphique d'un segment de l'orogène hercynien: les Cévennes médianes, Massif Central français. C R Acad Sci Paris 291:605–608

Miller CF (1985) Are strongly peraluminous magmas derived from pelitic sedimentary sources? J Geol 93:673–689

Montana A, Brearley M (1989) An appraisal of the stability of phlogopite in the crust and the mantle. Am Mineral 74:1–4

Montel JM, Weber C, Pichavant M (1986) Biotite-sillimanite-spinel assemblages in high-grade metamorphic rocks: occurrences, chemographic analysis and thermobarometric interest. Bull Mineral 109:555–573

Nekvasil H (1988) Calculated effect of anorthite component on the crystallization paths of H_2O-undersaturated haplogranitic melts. Am Mineral 73:966–981

Nekvasil H, Burnham CW (1987) The calculated individual effects of pressure and water content on phase equilibria in the granite system. In: BO Mysen (ed) Magmatic processes: physicochemical principles. Geochem Soc Spec publ 1:433–445

Patiño Douce A, Johnston AD (1991) Phase equilibria and melt productivity in the pelitic system: implications for the origin of peraluminous granitoids and aluminous granulites. Contrib Mineral Petrol 107:202–218

Perkins III D, Holland TJB, Newton RC (1981) The Al_2O_3 contents of enstatite in equilibrium with garnet in the system MgO-Al_2O_3-SiO_2 at 15–40 kbar and 900°–1110°C. Contrib Mineral Petrol 78:99–109

Perkins EH, Brown TH, Berman RG (1986) PTX-SYSTEM: three programs for calculation of pressure - temperature -composition phase diagrams. Comput Geosci 12:749–755

Peterson JW, Newton RC (1989) Reversed experiments on biotite-quartz-feldspar melting in the KMASH: implications for crustal anatexis. J Geol 97:465–485

Pettijohn FJ (1963) "Data of geochemistry, chap. S., chemical composition of sandstones – excluding carbonate and volcanic sands". US Geol Surv Prof Pap 440-S

Pin C, Duthou JL (1990) Sources of Hercynian granitoids from the French Massif Central: inferences from Nd isotopes and consequences for crustal evolution. Chem Geol 83:281–296

Pin C, Vielzeuf D (1983) Granulites and related rocks in Variscan median Europe: a dualistic interpretation. Tectonophysics 93:47–74

Robertson JK, Wyllie PJ (1971) Rock-water systems with special reference to the water-deficient region. Am J Sci 271:252–277

Rutter MJ, Wyllie PJ (1988) Melting of vapour-absent tonalite at 10 kbar to simulate dehydration-melting in the deep crust. Nature 331, 6152:159–160

Schmid R, Wood BJ (1976) Phase relationships in granulitic metapelites from the Ivrea-Verbano Zone (Northern Italy). Contrib Mineral Petrol 54:255–279

Seck HA (1971) Koexistierende Alkalifeldspäte und Plagioklase im System $NaAlSi_3O_8$-$KalSi_3O_8$-$CaAl_2Si_2O_8$-H_2O bei Temperaturen von 650°C bis 900°C. Neues Jahrb Mineral Abh 115:315–345

Segnit RA, Kennedy GC (1961) Reactions and melting relations in the system muscovite – quartz at high pressures. Am J Sci 259:280–287

Skjerlie KP, Johnston AD (1992) Vapor-absent melting at 10 kbar of a biotite- and amphibole-bearing tonalitic gneiss: implications for the generation of A-type granites. Geology 20:263–266

Skjerlie KP, Johnston AD (1994) Fluid-absent melting behaviour of a F-rich tonalitic gneiss at mid crustal pressures: implications for the generation of anorogenic granites. J Petrol (in press)

Thompson AB (1982) Dehydration melting of pelitic rocks and the generation of H_2O-undersaturated granitic liquids. Am J Sci 282:1567–1595

Vielzeuf D, Clemens JD, Pin C, Moinet E (1990) Granites, granulites, and crustal differentiation. In: Vielzeuf D, Vidal Ph (eds) Granulites and crustal evolution. Kluwer academic publishers, Dordrecht Boston London, pp 59–85

Vielzeuf D, Clemens JD (1992) The fluid-absent melting of phlogopite + quartz: experiments and models. Am Mineral 77:1206–1222

Vielzeuf D, Montel JM, Provost A, Kryza R (1991) The biotite - garnet - plagioclase - quartz assemblage as a potential geobarometer. EOS Trans Am Geophys Union 72, 44:559

Vielzeuf D, Holloway JR (1988) Experimental determination of the fluid-absent melting relations in the pelitic system. Contrib Mineral Petrol 98:257–276

Vielzeuf D (1984) Relations de phases dans le faciès granulite et implications géodynamiques. L'exemple des granulites des Pyrénées. Thèse Doctorat d'Etat, Clermont-Ferrand

Waters DJ (1988) Partial melting and the formation of granulite facies assemblages in Namaqualand, South Africa J Metamorphic Geol 6:387–404

Weber C, Barbey P (1986) The role of water, mixing processes and metamorphic fabric in the genesis of the Beaume migmatites (Ardèche, France). Contrib Mineral Petrol 92:481–491

Whetten JT, Kelley JC, Hanson LG (1969) Characteristics of Columbia River sediment and sediment transport. J Sediment Petrol 39:1149–1166

White AJR, Chappell BW (1988) Some supracrustal (S-type) granites of the Lachlan Fold Belt. Trans R Soc Edinburgh Earth Sci 79:169–181

Whitney JA (1975) The effects of pressure, temperature, and X_{H20} on phase assemblage in four synthetic rock compositions. J Geol 83:1–31